

**University of Mumbai**

## **Design of Rover**

Submitted in partial fulfilment of requirements  
for the degree of

**Bachelors in Technology**

by

**Vidhi Gohel**

**Roll No: 1812019**

**Vistasp Edulji**

**Roll No: 1815015**

**Atharva Makarand Pradhan**

**Roll No: 1815050**

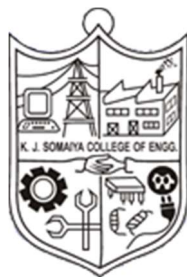
**Nirav Reshamwala**

**Roll No: 1815111**

Guide

**Dr. Sangita Bansode**

**Prof. Arati Phadke**



**Department of Mechanical Engineering &  
Department of Electronics Engineering  
K. J. Somaiya College of Engineering, Mumbai-77  
(Autonomous College Affiliated to University of Mumbai)  
Batch 2018 -2022**

# **K. J. Somaiya College of Engineering, Mumbai-77**

(Autonomous College Affiliated to University of Mumbai)

## **Certificate**

This is to certify that the dissertation report entitled **Design of Rover** submitted by Vidhi Gohel, Vistasp Edulji, Atharva Makarand Pradhan, Nirav Reshamwala at the end of semester VIII of LY B. Tech is a bona fide record for partial fulfilment of requirements for the degree of Bachelors in Technology in Mechanical Engineering of University of Mumbai

---

Guide

---

Guide

---

Head of Department

---

Principal

Date:

Place: Mumbai-77

**K. J. Somaiya College of Engineering, Mumbai-77**

(Autonomous College Affiliated to University of Mumbai)

**Certificate of Approval of Examiners**

We certify that this dissertation report entitled **Design of Rover** is bona fide record of project work done by Vidhi Gohel, Vistasp Edulji, Atharva Makarand Pradhan, Nirav Reshamwala during semester VIII. We certify that this dissertation report entitled **Design of Rover** is bona fide record of project work done by Vidhi Gohel, Vistasp Edulji, Atharva Makarand Pradhan, Nirav Reshamwala during semester VIII.

This project work is submitted at the end of semester VIII in partial fulfilment of requirements for the degree of Bachelors in Technology in Mechanical Engineering of University of Mumbai.

---

Internal Examiner

---

Internal Examiner

---

External/Internal Examiners

Date:

Place: Mumbai-77

**K. J. Somaiya College of Engineering, Mumbai-77**  
(Autonomous College Affiliated to University of Mumbai)

**DECLARATION**

We declare that this written report submission represents the work done based on our and / or others' ideas with adequately cited and referenced the original source. We also declare that we have adhered to all principles of intellectual property, academic honesty and integrity as we have not misinterpreted or fabricated or falsified any idea/data/fact/source/original work/matter in my submission.

We understand that any violation of the above will be cause for disciplinary action by the college and may evoke the penal action from the sources which have not been properly cited or from whom proper permission is not sought.

<div>Signature of the Student</div> <div>Roll No. 1812019</div>	<div>Signature of the Student</div> <div>Roll No. 1815015</div>
<div>Signature of the Student</div> <div>Roll No. 1815050</div>	<div>Signature of the Student</div> <div>Roll No. 1815111</div>

**Date:**

**Place: Mumbai-77**

## **Abstract**

A mobile platform that integrates various sensors onboard and traverses' adverse conditions has many unique applications. Often it is not safe to explore a region without compromising human safety. In such cases, robots are an alternative to traverse such environments and relay back data. A wheeled robot that can traverse such terrain and be suitable for the task at hand takes the form of a rover. This report presents the design of a six-wheeled rover with the capabilities of semi-autonomous navigation, remote sensing, and data transmission to aid in monitoring such locations. The rover utilizes stereo cameras to enable obstacle avoidance algorithms to permit autonomous maneuvering, without the prior mapping of the region. Arduino board controls and interfaces with various sensors. A higher-level microprocessor in the form of Raspberry Pi 4 performs obstacle detection and navigation. This design is validated through a prototype that successfully demonstrated the working of the various sub-systems, that constitute the rover.

**Key words:** Autonomous Navigation, Mobile Platform, Rover, Sensors, Mobile Robot.

# Table of Contents

<b>Abstract.....</b>	<b>iv</b>
<b>List of Figures.....</b>	<b>vii</b>
<b>List of Tables .....</b>	<b>viii</b>
<b>List of Equations .....</b>	<b>viii</b>
<b>Nomenclature .....</b>	<b>ix</b>
<b>1. Introduction .....</b>	<b>1</b>
1.1 Background .....	1
1.2 Scope of the Project.....	1
1.3 Organization of the Report .....	2
<b>2. Literature Survey .....</b>	<b>3</b>
<b>3. Methodology .....</b>	<b>9</b>
3.1 System Block Diagram.....	9
3.2 Physical Design .....	10
3.2.1 Outer Design.....	10
3.2.2 FEA Analysis.....	11
3.2.3 Driveline and Suspension .....	18
3.2.4 Motor Selection .....	19
3.3 Control and Navigation .....	20
3.3.1 Control Circuits .....	20
3.3.2 Navigational Algorithm.....	24
3.3.3 Stereo Image Computation .....	26
3.4 Power and Thermals.....	29
<b>4. Implementations and Results .....</b>	<b>30</b>
4.1 Physical Design of Prototype .....	30
4.2 Working of the Prototype.....	32
4.3 Control Board, Equipment and Sensor selection .....	34

4.4 Challenges during prototyping .....	35
4.4.1 Compass heading changing with orientation.....	36
4.4.2 Flexure of the prototype during first assembly.....	38
4.4.3 Powering Servo's from the 12V battery .....	38
4.4.4 Ineffective Speed Control.....	39
4.4.5 Loss of servo power during rover operation.....	40
4.4.6 Stereo Camera defective manufacturing.....	40
<b>5. Conclusions .....</b>	<b>41</b>
5.1 Conclusions and results.....	41
5.2 Further Work .....	42
<b>References.....</b>	<b>43</b>
<b>Appendix.....</b>	<b>46</b>

## List of Figures

Figure 3.1: Rover Block Diagram.....	9
Figure 3.2: Body structure of rover .....	11
Figure 3.3: Jigsaw pattern on the body parts .....	11
Figure 3.4 Acrylic Material Properties .....	12
Figure 3.5 Meshing of Body .....	13
Figure 3.6 Loading Conditions .....	13
Figure 3.7 Results of FEA of Body .....	14
Figure 3.8 Meshing of Rocker Bogie.....	15
Figure 3.9 Loading Conditions Forward Motion.....	15
Figure 3.10 Results of FEA of Rocker-Bogie Forward Motion .....	16
Figure 3.11 Loading Conditions Reverse Motion.....	17
Figure 3.12 Results of FEA of Rocker Bogie Reverse Motion .....	17
Figure 3.13: Design of Rocker-bogie mechanism .....	18
Figure 3.14: Free body diagram of a vehicle accelerated uphill.....	19
Figure 3.15: Block Diagram showing the various components and their interactions .....	21
Figure 3.16: Circuit Diagram of Driving Board. ....	22
Figure 3.17: Driving board block diagram .....	22
Figure 3.18: Control Board Circuit Diagram.....	23
Figure 3.19: Remote Board Circuit Diagram.....	24
Figure 3.20: Navigation algorithm for rover semi-autonomous navigation .....	25
Figure 3.21 Obstacle Avoidance Algorithm .....	26
Figure 3.22 Setup to capture reference image .....	27
Figure 3.23 Disparity Map of Reference Image .....	28
Figure 3.24 Electrical flow diagram .....	29
Figure 4.1: Physical Prototype of Rover.....	30
Figure 4.2: Laser Cut acrylic parts of the rover .....	31
Figure 4.3: Prototype Suspension .....	32
Figure 4.4: Raspberry Pi and OpenCV logos.....	33
Figure 4.5 Compass heading calculation .....	36
Figure 4.6: Pitch and Roll corrected values for heading calculation .....	36
Figure 4.7 Set-up for Magnetometer calibration.....	37
Figure 4.8: Flexure of parts during pre-assembly .....	39



Figure 4.9: Final bot without flexure .....	38
Figure 4.10: LM2569 Buck DC-DC Converter .....	39

## List of Tables

Table 3.1: Manufacturing costs for various materials .....	10
Table 3.2: Weight distribution of the Rover .....	12
Table 3.3: Weight Distribution of Electronic Components .....	12
Table 3.4: Summary of FEA of Body .....	14
Table 3.5: Summary of FEA of Rocker-Bogie Forward Motion .....	16
Table 3.6: Summary of FEA of Rocker-Bogie Reverse Motion .....	18
Table 4.1: Electronic Components and its specifications .....	34

## List of Equations

Equation 3.1: Torque equation.....	19
Equation 3.2: Relation between total vector travelled w.r.t individual vectors from IMU data .....	25
Equation 3.3: Relation between target, current and required vectors .....	26
Equation 4.1: Equations for pitch/roll corrected heading .....	37

## Nomenclature

$T_{req}$	Torque required to move the rover
$m$	Mass of the rover (kg)
$r$	Radius of rover wheel (m)
$g$	Acceleration due to gravity ( $m/s^2$ )
$\mu$	Co-efficient of friction
$\theta$	Incline Angle
$a$	Acceleration of the rover ( $m/s^2$ )
$q$	Position of Robot
$q_r$	Target Location
$V_0$	Interactive Potential
$V_n$	Interactive Potential
$c_1$	Positive constants
$c_2$	Positive constants

# Chapter 1

## Introduction

*This chapter introduces the background of the project and the motivations behind undertaking the project. It defines the scope of the project and outlines the report*

### 1.1 Background

It is sometimes risky to observe in person the conditions of an area, in times like these a mobile platform capable of relaying accurate data of a location can serve as an essential tool in decision making. A rover is a mobile platform that can navigate autonomously and can carry sensors that relay data back to a human controller.

Some extreme environments like the poles of the planet are too harsh for human observation over an extended period due to its varied environment. In such environments a rover can serve as platform for scientific measurement, aiding data gathering and remote observation of areas over a long period of time without need for human presence. Alternatively, climate change is causing devastating effects on the ecological environment of the planet [1]. This not only makes harsh environments such as the Arctic and Antarctic even harsher, but also increases the risk of extreme weather events on the planet [2]. In certain regions like Europe, it is estimated that around two-thirds of the population will be at risk of exposure to an extreme weather event by 2100 [3]. During times of catastrophe, post evacuation of an area, it is important to ascertain the damage and the safety of an area before allowing people to return to the location.

In all of the above cases, a rover can serve as a surveyor, quantifying the risks that can pose a hazard to the people that would move into those areas, and mitigating the chances for injury due to the same.

### 1.2 Scope of the Project

The main aim of the project is to design a functional prototype for a mobile remote sensing platform capable of monitoring and transmitting real time data of its surroundings. This takes the form of rover capable of semi-autonomous navigation and various sensors integrated onto it with transmission capability to a main hub.

Thus, the project's main objectives are listed as

- Design a rover capable of traversing complex terrain such as loose gravel, grass or debris.
- Employ sensors that collect environmental data
- Use a communication system such as RF to transmit and receive the data at a remote location
- Create an algorithm to navigate to a target location autonomously and avoid obstacles
- Study the possibility of integrating solar powered power systems

### **1.3 Organization of the Report**

The following report is divided into 5 chapters each covering different subtopics of the project. These subtopics separate the various systems that make up the robot. All chapters and their subtopics are listed in the table of contents, with each topic being hyperlinked for quick access.

- Chapter 1, defines the problem statement and the motivation behind choosing the topic.
- Chapter 2, provides a complete and coherent summation of the literature surveyed for the project, to make assumptions and conclusions that drove design decisions.
- Chapter 3, is used to explain the decisions made during the design process, with regards to part selection, how each component is analyzed and how the algorithms were chosen.
- Chapter 4, provides the details of the implementation of various sub-systems and how they were altered to meet requirements that arose due to the nature of the problem at hand.
- Chapter 5, provides a quick and precise summary of project fulfillment and the state of the project as of the writing of this report. This chapter also discusses further improvements that can be made to improve upon the present iteration.

## Chapter 2

### Literature Survey

*This chapter presents a comprehensive review of various technologies that have been utilized in past rover designs.*

To understand the various design possibilities and the requirements of rover technologies a thorough review of the various literature available on various rover designs used in applications was conducted. Since the rover application originated from space programs several contributions to the survey are a direct result of the work done at NASA. Presently, there are multiple rover systems for both extra-terrestrial and terrestrial terrains. Many concepts from these extra-terrestrial rovers can be extrapolated for terrestrial rovers.

James Zakrajsek *et al.* [4] have given an overview of various existing extra-terrestrial rover models with their specifications like speed, distance travelled along with the challenges associated with each. They also describe a few conceptual rover models proposed since the initial rover models. Bickler [5], in his study, states that among a variety of configurations for rovers the wheeled rovers offer the most simplicity of all possible configurations. In addition, his study found that a 6 wheeled rover, with the corner 4 steerable offers the most optimum configuration between trade-offs of weight, maneuverability, and obstacle avoidance capability of the rover. The corner steering, with each wheel, independently actuated allows for the rover to bring its steering point to the center allowing for it to turn in place. It also utilized a Rocker-Bogie system as its suspension. After further development at NASA, Lindemann, *et al.* [6] note that the Rocker-Bogie configuration allows for passively keeping each wheel in contact with the terrain. This provides the advantage of evenly spreading out the load across all 6 wheels preventing the wheels from sinking into the ground due to the weight being concentrated on one. During rough terrain, an additional advantage of this design is that it allows all 6 wheels to grip the surface for maximum possible traction by utilizing a driving actuator on each wheel. There are also certain alternatives to the Rocker-Bogie mechanism like Abin Simon *et al.* [7] present the design of spider mechanism that enables the arms of the rover to traverse up stepped terrain and able to absorb the shocks without damaging the rover. They performed kinematics and dynamic analysis on ADAMS and validated the design using a prototype.

Many rover models were developed to help in research for new and better technologies. Hans P. Moravae [8] developed a rover called the CMU Rover which was a camera-equipped mobile

robot. This robot was built to aid research in sensing, perception, control, and planning. For traversing in an extreme environment, it is necessary to validate that the rover will work seamlessly in those conditions. Sanjiv Singh *et al.* [9] developed a rover that uses both global and local navigational schemes that evaluate the travers ability to autonomously navigate the rover. The developed rover uses a single processor for all sensing and decision making. The authors discuss overall system architecture and result from simulation as well as experiments. R. Lagisetty *et al.* [10] developed real-time obstacle detection and obstacle avoidance for autonomous navigation in unstructured environments using stereo cameras. They simulated and validated obstacle detection using a stereo camera and pose estimation using feature tracking. Xujung Guan *et al.* [11] propose a navigational algorithm based on Strapdown Inertial Navigational System (SINS) using star sensors for determining the rover's position and attitude. They divided the method into two parts where firstly, there is coarse alignment and navigation which gives an approximate position and attitude. In the second part, there is a fine adjustment in the position and attitude to increase the accuracy. They simulated this model and compared it with pure inertial navigation. The simulation results depicted that the model was able to achieve high accuracy.

Simulation plays a key role to develop a rover. This helps to validate the design, reduce the risk of failure, and helps increase the accuracy of the system. Jeng Yen [12] presents ROAMS software which is software for real-time simulation of mobile robotic vehicles, so provides a virtual testing ground for subsystems. This software could simulate mechanical subsystems, electrical subsystems, internal and external sensors, and onboard control software. Further, the author also discusses the integration of this software with planning software. J.Y. Wong [13] proposed a practical methodology to predict performance on rover wheels on other planets based on the tests performed in simulated conditions. The rigid wheel sinkage on Lunar soil simulants and Toyoura sand was tested and from this experiment was compared with test data. J.Y Wong *et al.* [14] provided further evidence to substantiate the merits of the previous work. It was concluded that gravity has trivial effect on the slip and sinkage of rover wheels.

Tim Hojnik *et al.* [15] propose a posable wheel hub design for terrestrial and extra-terrestrial exploration. The wheel hub has the capability of self-recovery if the rover gets stuck. It uses electric actuators that enable the position of the wheel hub center to be manipulated. The authors performed experiments using a four-wheeled rover having posable hubs and compared the results of debugging, chassis levelling, and generating locomotion using potential energy in case of failed motor drive with classical wheels and conclude that the posable hubs are much

better suited for unstructured terrain. Eisen *et al.* [16], describe the actuator for the mobility of the rover as a brushed DC motor for the rover. The DC motor was selected for its simplicity to control and minimum wiring required to prevent heat loss. The motor was attached to a 5-stage planetary gearbox of ratio 2000:1. The rover utilized a combination of LED and photoresistor as a 1-bit encoder for motor odometry. The steering assembly also used the same actuator but omitted the LED-photoresistor pair as it used a conductive plastic potentiometer on the output bevel gear to measure the steering angle. The wheels used a magnetic detent clutch to prevent wheels from slipping.

Eisen *et al.* [17], describe the Warm Electronics Box (WEB) of the Sojourner rover as a fiberglass epoxy sheet and spar walls lined with Silica Aerogel as insulation. Additionally, three RHU (Radioisotope Heater Units) were used as sources of heat. Roncoli *et al.* [18], describe the structure of the MER rover body and primary structure, also called the WEB, as an exoskeleton of composite honeycomb lined with silica aerogel for insulation. The WEB houses all the electronics of the including the control computer, batteries, and communication hardware. Novak *et al.* [19], further elaborate on the thermal design by specifying that the honeycomb is made of aluminium lined with carbon composite face sheets. The silica gel used in the insulation had been carbon opacified to block infrared thermal transmission. Both the internal and external surfaces were covered in co-cured goldized Kapton that had a low emissivity surface finish to minimize radiation losses. To prevent heat loss from wires, FlexPrint cabling (copper traces clad onto a polyimide base) was used instead. In addition, the cables were run through tunnels insulated with rigid polyurethane foam that kept the insulation up to 0.5 m into the web before egress. All major masses in the web were supported with thin-walled tubular struts with Ti fittings. The struts were fabricated using Boron/Epoxy and glass/epoxy materials. Bhandari *et al.* [20], describe the heat control architecture of the MSL rover. The MSL rover due to its different source of energy, namely an RTG was able to leverage the waste heat radiated by it and use it in a single-phase heat exchanger to regulate the temperature of the rover. Using a set of control valves to regulate itself. The rover would transfer heat from the RTG to the electronics or from the electronics to the cold plate/radiator to maintain the narrow band of temperature required for the electronics to survive.

For the Selection and designing of the solar panel various references, considerations and many problem statements were found. Reviewing many papers and books has helped with coming up of solution. Stella *et al.* [21] the author has briefly provided information about the solar panel integration with the Mars Exploration Rovers (MER) and with the carrying cruise shuttle

of the rovers. The panel Arrays were designed differently for both same and a proposition of using solar triple junction cells instead of standard GaAs cells was tossed. The rover array of solar panel consisted of 5 deployable and 1 fixed solar array. Pazar [22] in his studies observes the difference in solar irradiance of the Earth and that of Mars and reduces the incident irradiance factor accordingly. Vertat and Vobornik, [23] Designs the solar panels for a CubeSat Picosatellite, where he suggests that by making the panels deployable the power output can be increased by approximately 4.5W ( $7.04-2.47=4.57$ ). For the storage of the generated power the author, TINA *et al.* [24] uses batteries for the DC current storage and supply to the circuit boards, and uses capacitor to store AC current for the electric servo motors. Raza *et al.* [25] included a forecasting model like Artificial Neural Network (ANN) for forecasting of Photovoltaic power output with different variables which are varied factors affecting the photovoltaic power output of a particular site and the forecast error of the model was 7.04%. Different affecting factors they considered are air temperature, wind speed, solar irradiance. Bett and Thornton [26] conducts detailed analysis of relation between wind speed, irradiance and surface clearness on different days and different seasons throughout the entire year. Results are that the irradiance is inversely proportional to the wind speed and irradiance is directly proportional to the surface clearness. Islam *et al.* [4] has used the P-spice software and did various simulations of Solar PV output under different wavelengths of light that resulted into some useful insights. They first separated the wavelength range into 3 major useful sections that is UV, Visible and Infrared, based on the photon energy and the standard air mass was considered 1.5 (AM 1.5D). With the simulation results, the best wavelength range was of visible range (380-750 nm) hence a more detailed simulation analysis was done by further separating into distinct colors (VBGYOR) and all were compared to find out the best range of wavelength for maximum and efficient solar PV output. A plotted graph of wavelength versus irradiance showed that irradiance is maximum in the range of Visible spectrum. Vidyanandan [27] the author compared 3 types of the solar panels with different parameters and all the losses were presented in graphical manner. Parameters were degradation of PV module, variation of solar radiation, module temperature, fill factor, parasitic resistance, shading, soiling and covering, Potential Induced Degradation, PV Module Orientation and Tilt Angle and strong conclusions were drawn. Pervaiz and Khan [28] main objective was to understand the effects of low solar irradiance or for winter season. They calculated the losses per day as the variation of the peak sunlight hour, for example the losses were 3.8%, 4%, 4.5% for peak sunlight hours of 4.4, 4, and 3.4. The author states that a technique of shade- tolerant Maximum Power Point



Tracking (MPPT) mechanism and array reconnection to overcome partial shading issues. Khamisani [29] is designing an off-grid solar powered system for a site in a particular method. First the power usage is calculated then to go off-grid solar panel needs to produce equal power and according to that the solar panel sizing is done.

For the Selection and designing of the solar panel various references, considerations and many problem statements were found. Reviewing many papers and books has helped with coming up of solution. Stella *et al.* [21] the author has briefly provided information about the solar panel integration with the Mars Exploration Rovers (MER) and with the carrying cruise shuttle of the rovers. The panel Arrays were designed differently for both same and a proposition of using solar triple junction cells instead of standard GaAs cells was tossed. The rover array of solar panel consisted of 5 deployable and 1 fixed solar array. Pazar [22] in his studies observes the difference in solar irradiance of the Earth and that of Mars and reduces the incident irradiance factor accordingly. Vertat and Vobornik, [23] Designs the solar panels for a CubeSat Picosatellite, where he suggests that by making the panels deployable the power output can be increased by approximately 4.5W ( $7.04 - 2.47 = 4.57$ ). For the storage of the generated power the author, TINA *et al.* [24] uses batteries for the DC current storage and supply to the circuit boards, and uses capacitor to store AC current for the electric servo motors. Raza *et al.* [25] included a forecasting model like Artificial Neural Network (ANN) for forecasting of Photovoltaic power output with different variables which are varied factors affecting the photovoltaic power output of a particular site and the forecast error of the model was 7.04%. Different affecting factors they considered are air temperature, wind speed, solar irradiance. Bett and Thornton [26] conducts detailed analysis of relation between wind speed, irradiance and surface clearness on different days and different seasons throughout the entire year. Results are that the irradiance is inversely proportional to the wind speed and irradiance is directly proportional to the surface clearness. Islam *et al.* [4] has used the P-spice software and did various simulations of Solar PV output under different wavelengths of light that resulted into some useful insights. They first separated the wavelength range into 3 major useful sections that is UV, Visible and Infrared, based on the photon energy and the standard air mass was considered 1.5 (AM 1.5D). With the simulation results, the best wavelength range was of visible range (380-750 nm) hence a more detailed simulation analysis was done by further separating into distinct colors (VBGYOR) and all were compared to find out the best range of wavelength for maximum and efficient solar PV output. A plotted graph of wavelength versus irradiance showed that irradiance is maximum in the range of Visible spectrum. Vidyanandan

[27] the author compared 3 types of the solar panels with different parameters and all the losses were presented in graphical manner. Parameters were degradation of PV module, variation of solar radiation, module temperature, fill factor, parasitic resistance, shading, soiling and covering, Potential Induced Degradation, PV Module Orientation and Tilt Angle and strong conclusions were drawn. Pervaiz and Khan [28] main objective was to understand the effects of low solar irradiance or for winter season. They calculated the losses per day as the variation of the peak sunlight hour, for example the losses were 3.8%, 4%, 4.5% for peak sunlight hours of 4.4, 4, and 3.4. The author states that a technique of shade- tolerant Maximum Power Point Tracking (MPPT) mechanism and array reconnection to overcome partial shading issues. Khamisani [29] is designing an off-grid solar powered system for a site in a particular method. First the power usage is calculated then to go off-grid solar panel needs to produce equal power and according to that the solar panel sizing is done.

## Chapter 3

### Methodology

*This chapter presents the various methods and calculations followed to arrive at the design decision that have been made in order to fulfil the necessary problem statement*

The design of the rover consists of 3 separate categories. Each of which has its own sub categories that must be designed and tested. In this section of the report, the various design decisions used when making the rover as well as the idea behind the navigation algorithm used are described.

### 3.1 System Block Diagram

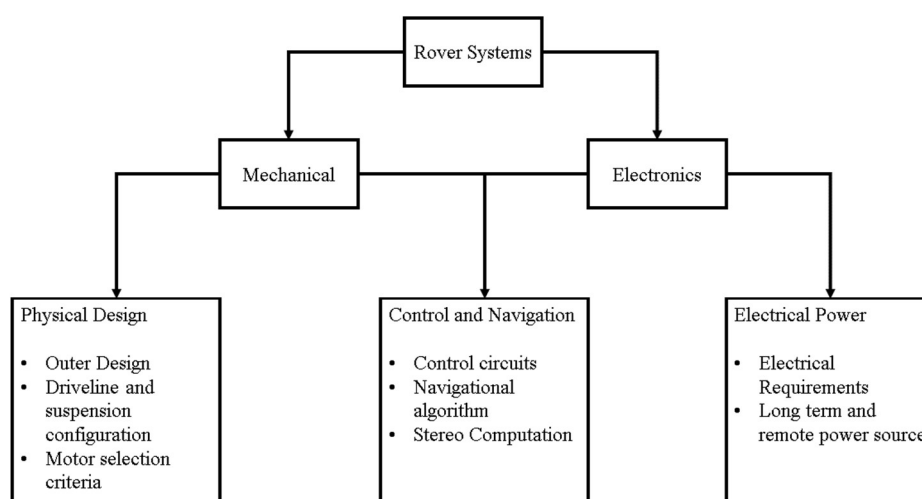


Figure 3.1: Rover Block Diagram

The rover design consists of three major categories.

- **Physical Design:** This category deals with design decisions pertaining to the selection of the configuration, the decisions behind what wheels to steer and what kind of suspension and motors to use.
- **Control and Navigation:** This category deals with the various circuits driving the rover sub-systems and their control. It also catalogues how data is synched between the various sub-systems and used to execute command decisions

- **Power and Thermals:** This category deals with managing the available electrical energy to ensure that all necessary components receive power as and when they require it. It also, briefly explores alternative power sources that can allow an extended range using renewable power as well as environmental considerations left out by the design.

## 3.2 Physical Design

The driveline consists of three major components the motor, the wheels and the suspension. Steering component is integrated with the suspension component.

### 3.2.1 Outer Design

The Rover Design was conducted using the SolidWorks CAD platform, since the suspensions to be used is a rocker-bogie mechanism, it would require flat surfaces to mount firmly with the body. Additionally, the use of stereo cameras would require a similar treatment. Hence a cuboidal shape was finalized for the main body of the bot. The floor area was finalized such that the differential of the rocker-bogie mechanism could be accommodated with ease.

In order to select the material for the rover a cost analysis of the manufacturing cost for various materials based on rough estimates of the required material was performed which is summarized in Table 3.1. The machining costs for aluminum include water jet cutting and for acrylic and ply they include laser cutting costs. Both methods were chosen on the basis of availability and speed of manufacturing

Table 3.1: Manufacturing costs for various materials

	<b>Aluminium</b>	<b>Acrylic</b>	<b>Pure Ply</b>	<b>Acrylic + Ply</b>
<b>Material Cost (in Rs)</b>	500	3600	2800	1800
<b>Machining cost (in Rs)</b>	2500	500	500	800
<b>Total Cost (in Rs)</b>	3000	4100	3300	2600

A common requirement during manufacturing of such parts is the need to use a jig/fixture to ensure alignment of the parts. This would increase the material required and thus the cost of the project. To avoid the problem, a jigsaw pattern that would allow the parts to snap together,

with tight tolerances, preventing the need for jigs or fixtures was implemented. Due to the light weight of the rover and limited loads on the structure, 3 mm acrylic was used as the material of choice, reinforced with ply where required.

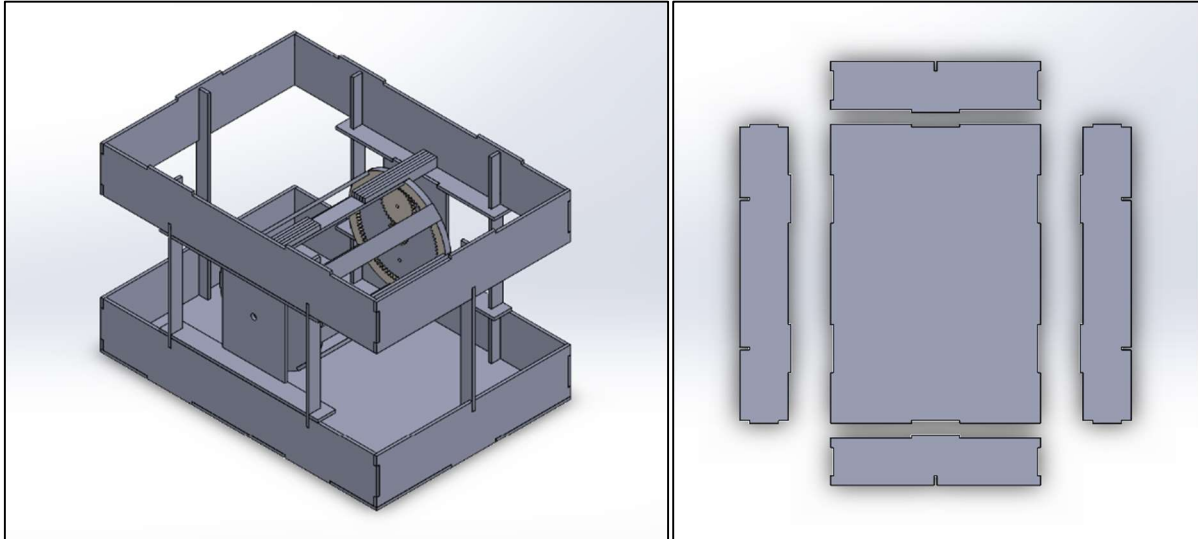


Figure 3.2: Body structure of rover    Figure 3.3: Jigsaw pattern on the body parts

The CAD design was built using 3mm acrylic and simulated using ANSYS Workbench for FEA analysis. The weight of the structure alone was estimated to about 950 grams from SolidWorks software.

### 3.2.2 FEA Analysis

The FEA analysis was used to analyze weak spots on the design. These weak spots were reinforced using ply and acrylic. FEA analysis of the body and the rocker bogie mechanism was performed on Ansys Workbench. The overall weight of the rover was estimated to 5 Kg. The estimation of unknown parts was done using SolidWorks software and for electronic components websites and datasheets were used. The partwise weight has been summarized below Table 3.2: Weight distribution of the Rover. Hence, the analysis was performed for two loads at 60N and 75N of load on the structure which corresponds to a factor of safety of 1.2 and 1.5 for the main structure.

Table 3.2: Weight distribution of the Rover

Part	Weight (grams)
Body	770
Rocker Bogie	180
Wheels	750
Electronics	2245.8
Miscellaneous Reinforcement	1000
<b>Total</b>	<b>4945.8</b>

Table 3.3: Weight Distribution of Electronic Components [30 - 39]

Electronics Part	Weight (grams)
Motors	900
Servo Motors	220
Raspberry Pi	46
Arduino	50
Battery	600
Power Bank	400
Buck Converter	11
Magnetometer + IMU + GPS Module + Temperature Sensor	$2 + 2.1 + 12 + 2.7 = 18.8$
<b>Total</b>	<b>2245.8</b>

Acrylic was used as the material for the analysis. Following are the material properties of acrylic used.








1	Property	Value	Unit
2	 Material Field Variables	 Table	
3	 Density	1180	kg m <sup>-3</sup> ▼
4	 Isotropic Elasticity		
5	Derive from	Shear Modulus... ▼	
6	Young's Modulus	4.658E+09	Pa
7	Poisson's Ratio	0.37	
8	Bulk Modulus	5.9718E+09	Pa
9	Shear Modulus	1.7	GPa ▼
10	 Tensile Yield Strength	74.1	MPa ▼
11	 Compressive Yield Strength	117	MPa ▼
12	 Tensile Ultimate Strength	72.5	MPa ▼

Figure 3.4 Acrylic Material Properties [40]

### 3.2.2.1 Body

FEA analysis of the body is performed and the deflection and equivalent stress are calculated to analyze the weak spots and apply appropriate reinforcement.

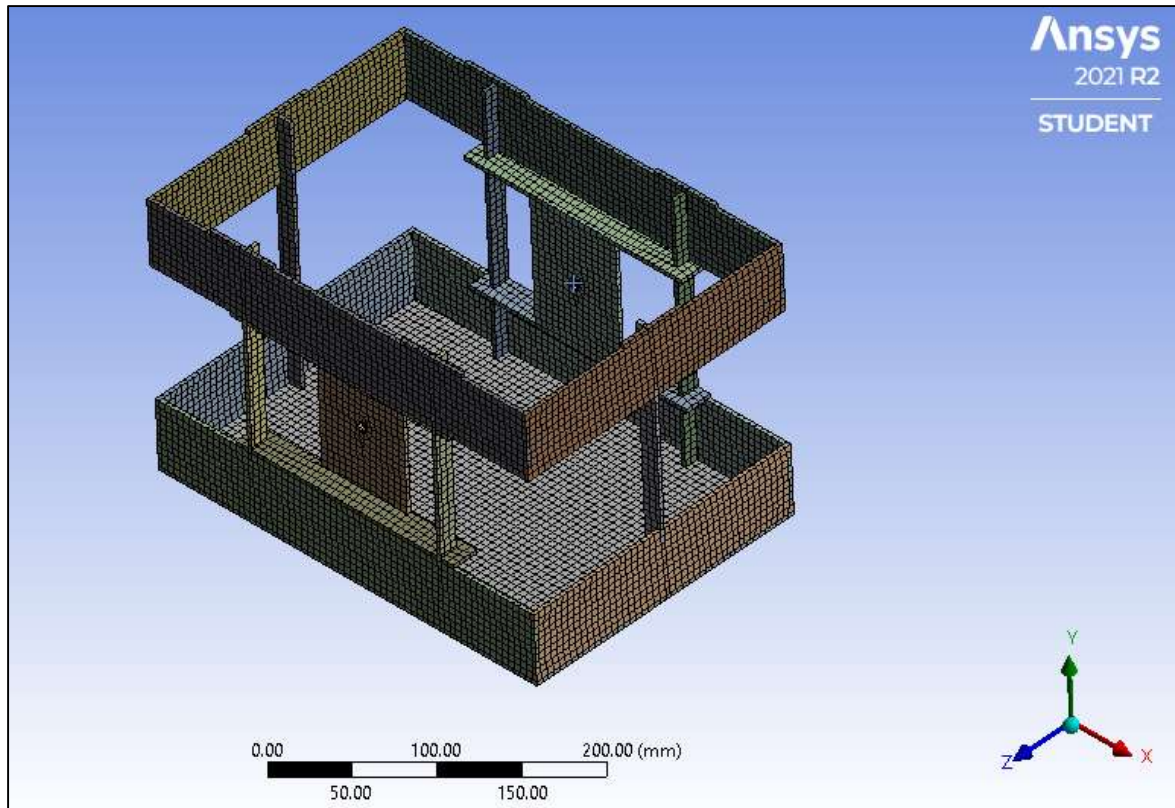


Figure 3.5 Meshing of Body

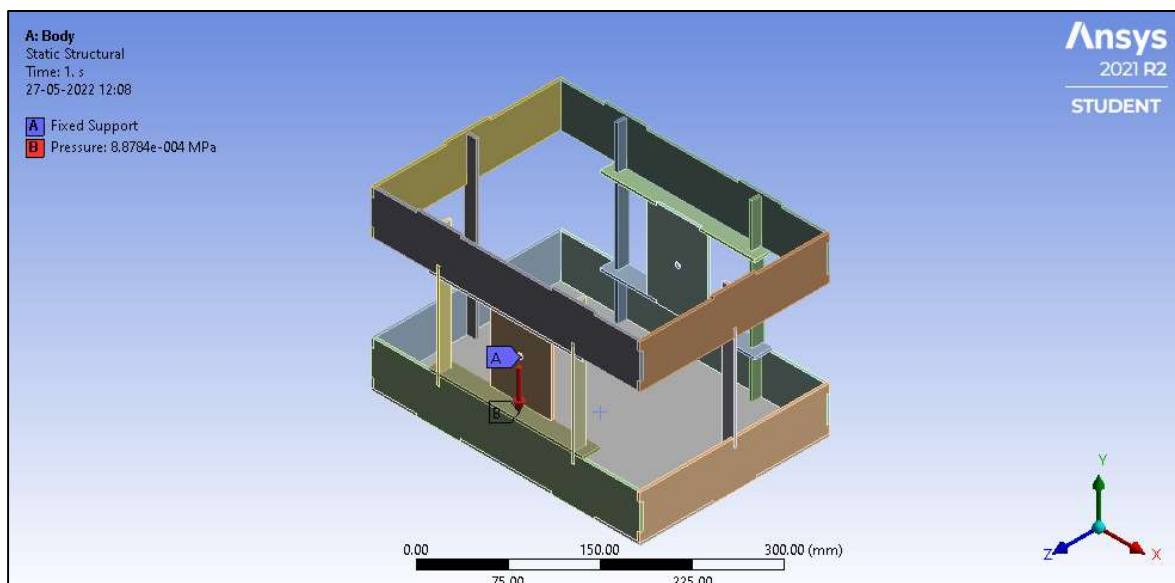
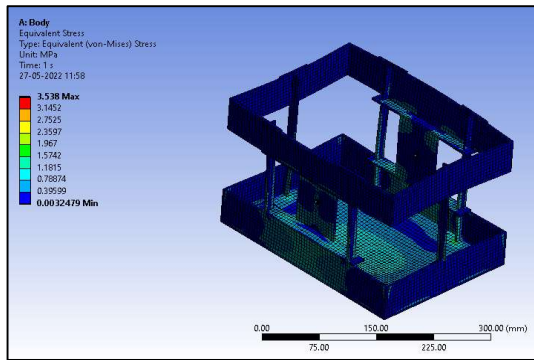
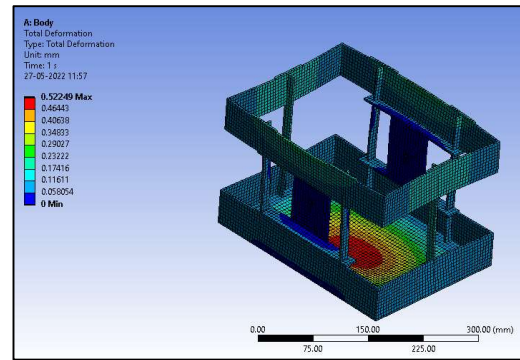


Figure 3.6 Loading Conditions

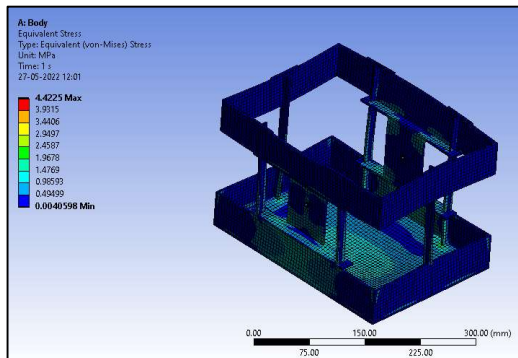




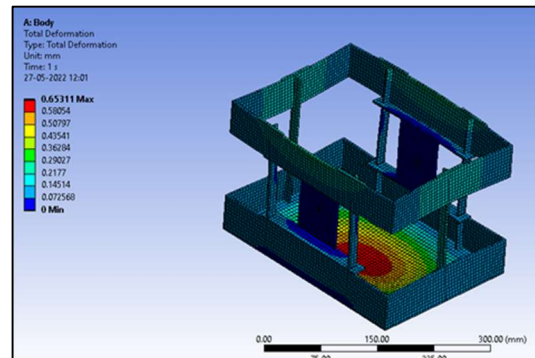
a) Equivalent Stress at 60N Load



b) Deformation at 60N Load



c) Equivalent Stress at 75N Load



d) Deformation at 75N Load

Figure 3.7 Results of FEA of Body

On comparing Table 3.4: Summary of FEA of Body and Figure 3.4 Acrylic Material Properties it can be concluded that the Body is safe under high loading. Also, the current weight of the Rover is about 5kg (Table 3.2: Weight distribution of the Rover) which is less than 60N.

Table 3.4: Summary of FEA of Body

Load	Equivalent Stress (MPa)		Deformation (mm)	
	Min	Max	Min	Max
60N	0.0033	3.5853	0	0.52954
75N	0.004	4.4822	0	0.66192



### 3.2.2.2 Rocker – Bogie

FEA analysis of the rocker-bogie system is performed and the deflection and equivalent stress are calculated to analyze the weak spots and apply appropriate reinforcement.

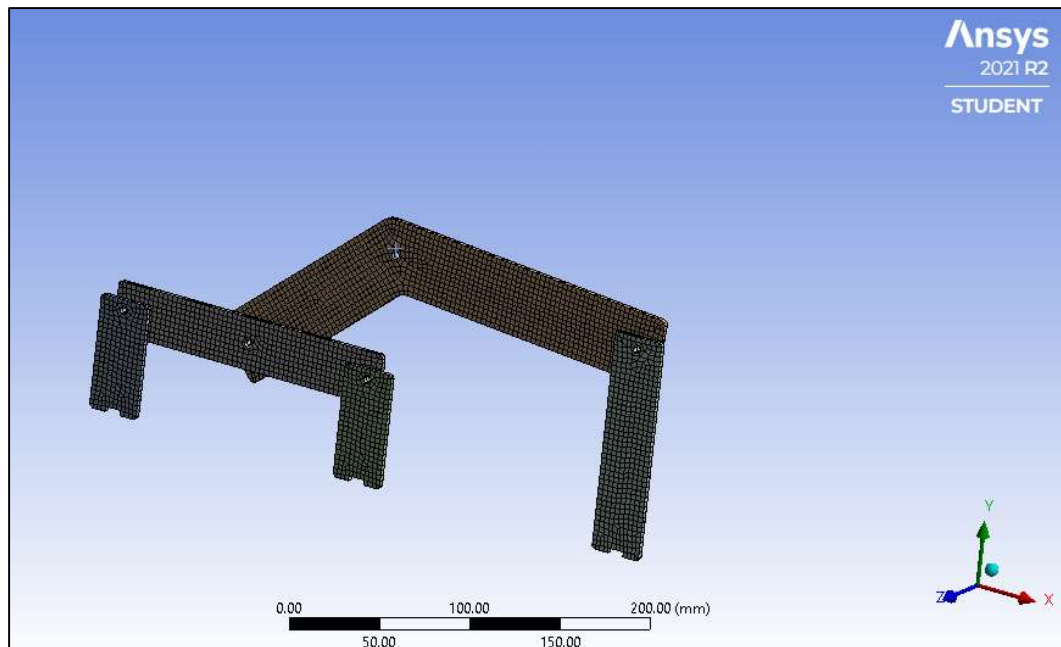


Figure 3.8 Meshing of Rocker Bogie

In the rocker-bogie mechanism moments due to motor are also considered hence, two cases namely forward and reverse case are considered.

- Forward Case: - In this case all the motors rotate in such a way that the rover moves in the forward direction.

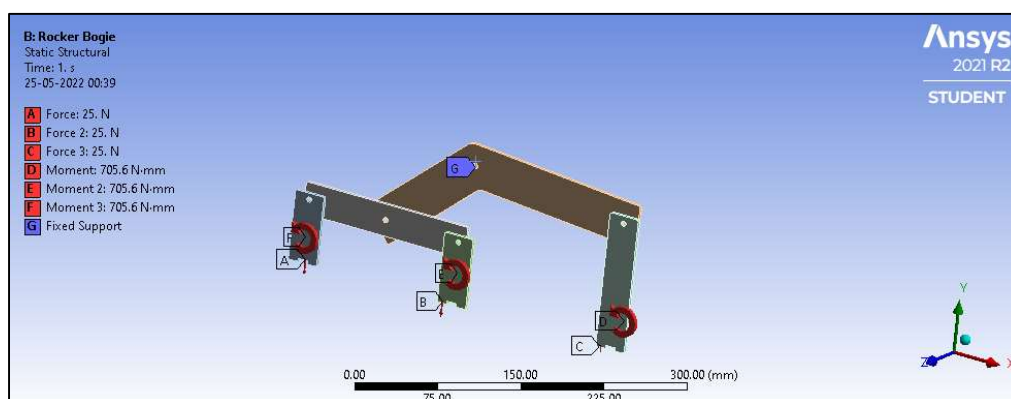
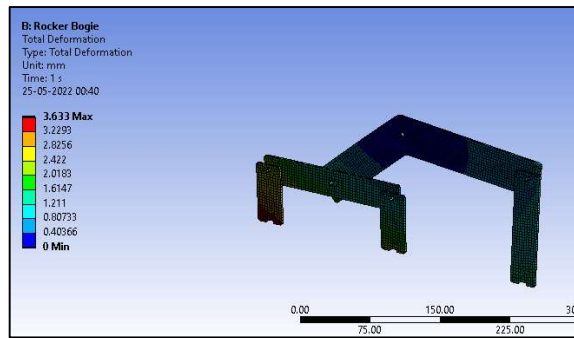
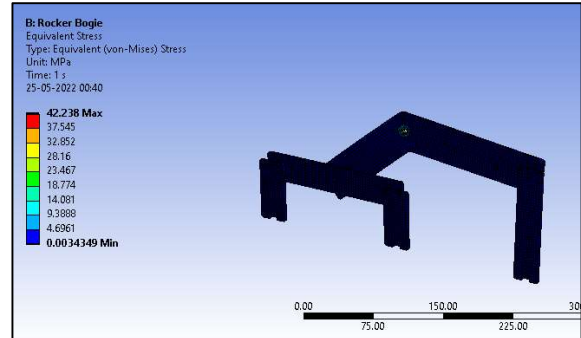


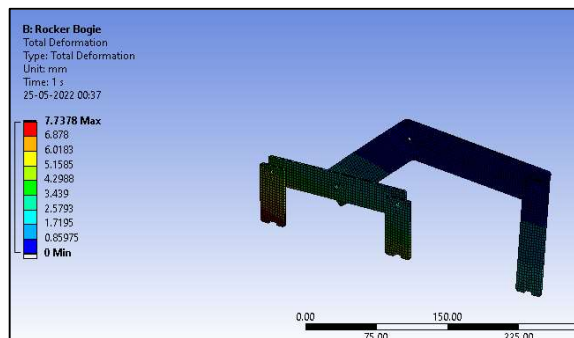
Figure 3.9 Loading Conditions Forward Motion



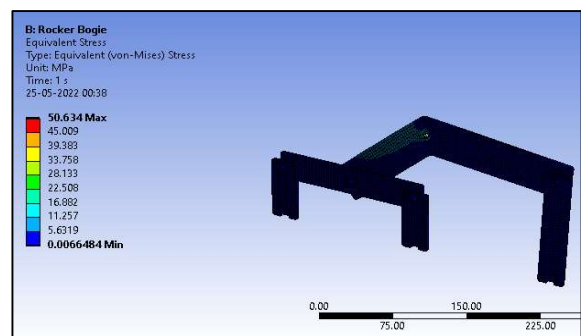
a) Deformation at 60N Load



b) Equivalent Stress at 60 N Load



c) Deformation at 75N Load



d) Equivalent Stress at 75N Load

Figure 3.10 Results of FEA of Rocker-Bogie Forward Motion

The results of the analysis conducted for the forward case are tabulated below.

Table 3.5: Summary of FEA of Rocker-Bogie Forward Motion

Forward	Equivalent Stress (MPa)		Deformation (mm)	
Load	Min	Max	Min	Max
60N	0.0034	42.238	0	3.633
75N	0.0066	50.643	0	7.7378

- Reverse Case: - In this case all the motors rotate in such a way that the rover moves in the reverse direction.

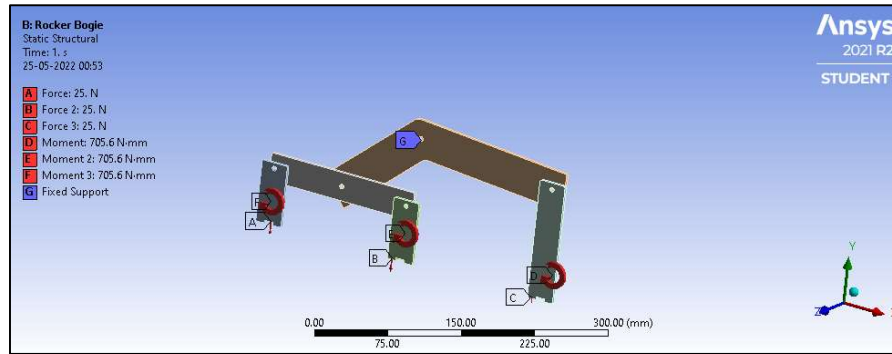
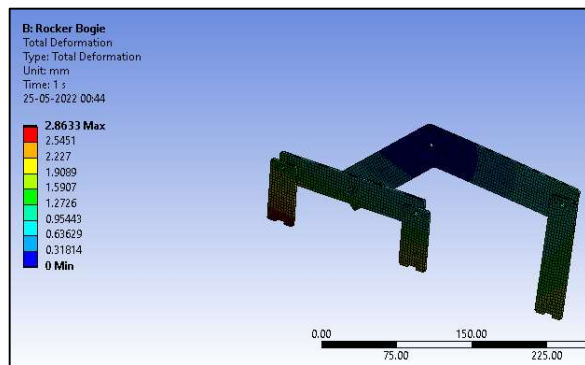
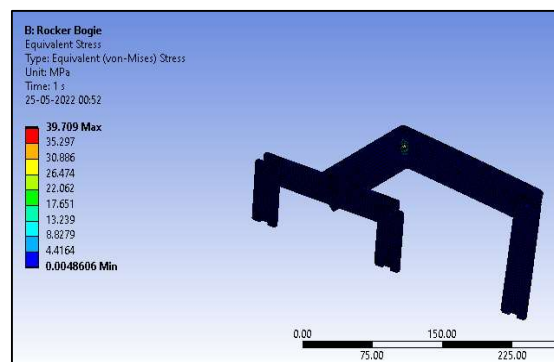


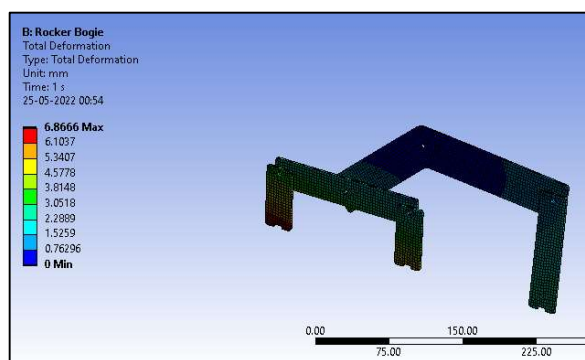
Figure 3.11 Loading Conditions Reverse Motion



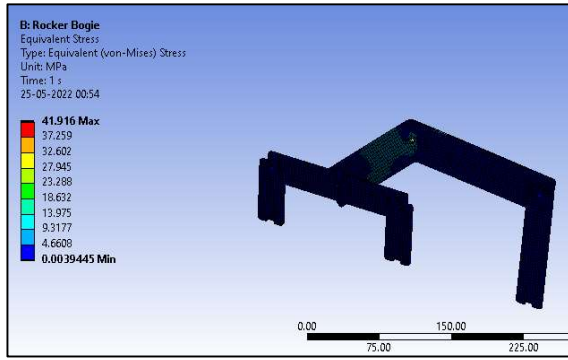
a) Deformation at 60N Load



b) Equivalent Stress at 60 N Load



c) Deformation at 75N Load



d) Equivalent Stress at 75N Load

Figure 3.12 Results of FEA of Rocker Bogie Reverse Motion

Hence, when Table 3.5: Summary of FEA of Rocker-Bogie Forward Motion and Table 3.6: Summary of FEA of Rocker-Bogie Reverse Motion are compared with Figure 3.4 Acrylic Material Properties it can be concluded that the Rocker-Bogie Mechanism is safe. Furthermore, as a precautionary measure ply reinforcement is also provided to the Rocker-Bogie.

Table 3.6: Summary of FEA of Rocker-Bogie Reverse Motion

Reverse	Equivalent Stress (MPa)		Deformation (mm)	
	Min	Max	Min	Max
60N	0.0048	39.709	0	0.52954
75N	0.0039	41.916	0	6.8666

### 3.2.3 Driveline and Suspension

The driveline represents the configuration of wheels and steering used in the rover. As discussed in the literature survey [5], 6 wheeled rovers with 4 corner steerable wheels provide the most optimum mixture of stability, maneuverability and complexity in terms of design. This is reinforced by various designs referenced in the literature adopting the same. Thus, the time-tested configuration of having 6 wheels, 3 on each side of the rover, driven independently is used for the rover. The corner 4 wheels are steerable and are coded such that their motion obeys the law of gearing for steering pairs.

The rover suspension consists of a rocker-bogie mechanism. The rocker-bogie mechanism ensures that all 6 wheels maintain contact with the ground surface, passively without any active suspension elements such as springs or shock absorbers. Although, this leads to a trade-off where the speed of the rover must be reduced to reduce the shock on the system. Chinchkar, *et al.* [41], have in their report outlined the methods and techniques required to graphically calculate the dimensions of the rocker bogie system. Having used the same to calculate the base dimensions required for the rover utilizing the SolidWorks software utility to ensure accuracy.

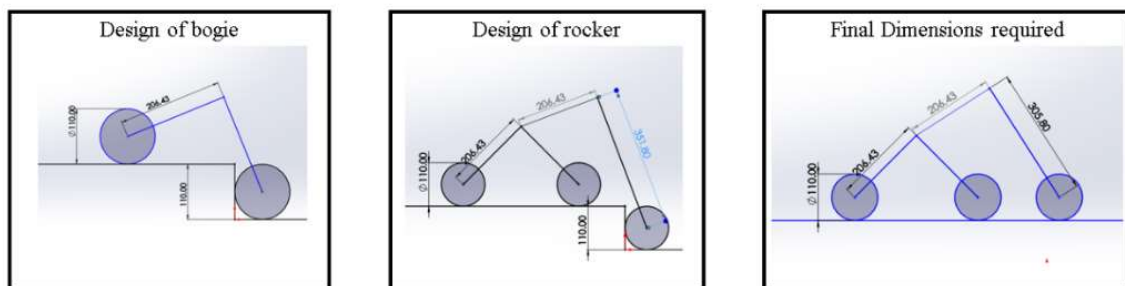


Figure 3.13: Design of Rocker-bogie mechanism

### 3.2.4 Motor Selection

Brushed DC Motors serve as the rover's main source of motion. They are vital components required to run the rover and provide the power necessary to ensure mission success and ensure that the project objectives are fulfilled.

To select the motors, Equations of powertrain kinematics and traction [42] for a four-wheeler were used and simplified as per the requirement of the rover to select the motors. Since the wheels are directly driven, the variables describing the transmission parameters were eliminated from the equation.

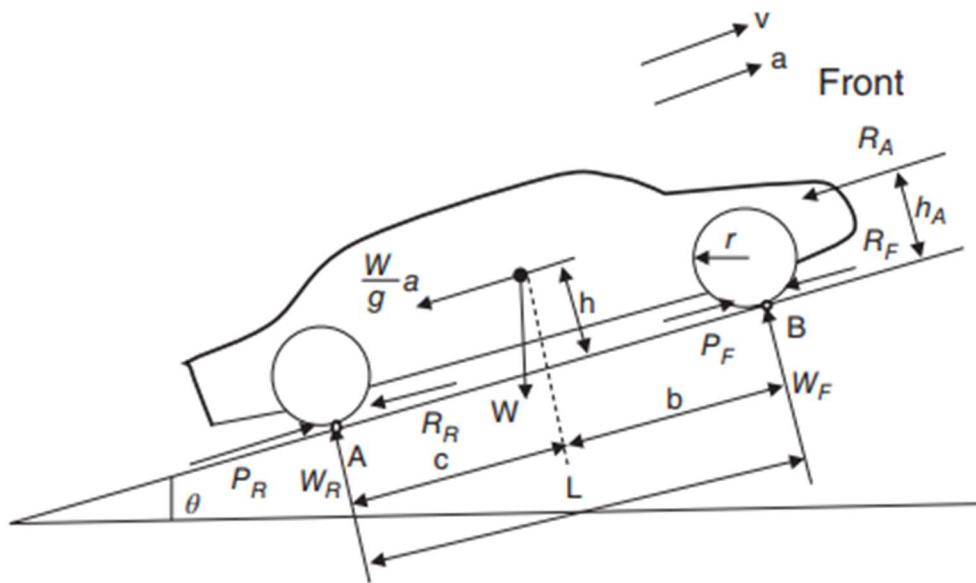


Figure 3.14: Free body diagram of a vehicle accelerated uphill

After simplifying the equation, following equation is obtained,

Equation 3.1: Torque equation

$$T_{req} = m * r * (g * (\mu + \sin \theta) + a)$$

To solve the equation the terms were selected using the following methods,

- **$\theta$  – Angle of Inclination:** The maximum incline that the rover will face is  $30^\circ$  as there is danger of tipping over beyond it.
- **$\mu$  – Coefficient of friction:** The co-efficient of friction was taken as 0.2 [43] as that is the lowest friction value for rubber wheels for various surfaces.

- **r – Radius of wheel:** The wheel radius is responsible for the size of obstacle that can be climbed. According to the literature surveyed, when used in conjunction with the rocker- bogie system a rover wheel can climb an obstacle half the diameter of the wheel i.e., the radius.
- **m – Mass of rover:** The mass of the rover is influenced by the scientific payload aboard, the material, insulation used and the size of the suspension. The size of the rover is dependent on the application. The smallest rover in literature had a footprint of 1m x 1.5m and the largest, ‘The Curiosity Rover’ is the comparable to the size of an SUV.
- **a – Acceleration of the rover:** The acceleration of the rover is influenced by the need to travel a certain speed and the dynamic loading caused on the structure. The acceleration is capped to prevent excessive dynamic loads on the structure.

Thus, based on above values the torque required for driving the rover for a range of masses can be calculated.

### 3.3 Control and Navigation

Control and Navigation delves into the details of the functional circuits that drive the functioning of the rover as well as the control algorithms that convert on-board data into control decisions. It also highlights the sensor data collection capabilities and how they are transmitted.

The rover follows a two-level microcontroller design. The lower-level micro-controllers are responsible for managing the working of the rover and handling the collection and transmission of data. The Arduino platform serves as the lower-level micro-controller. The higher-level micro-processors, are responsible for processing the stereo images and running the driving algorithm for semi-autonomous navigation.

#### 3.3.1 Control Circuits

Rover operations can be broken down into two fundamental tasks. The first is controlling and operating the various motors that drive the physical bot. The second can be interfacing various sensors, communication and decision making based upon the on-board data. These tasks are handled independently by an Arduino Uno Microcontroller board that can perform their individual work without relying on the other. A Raspberry Pi 4, running Linux is the central computational hub that processes the data from the sensor Arduino and commands and navigates the entire bot using both the on-board IMU and Stereo Vision. Sensor Data and

captured images are sent back via RF to a remote controller that is itself an Arduino Uno connected to a host PC via a serial port.

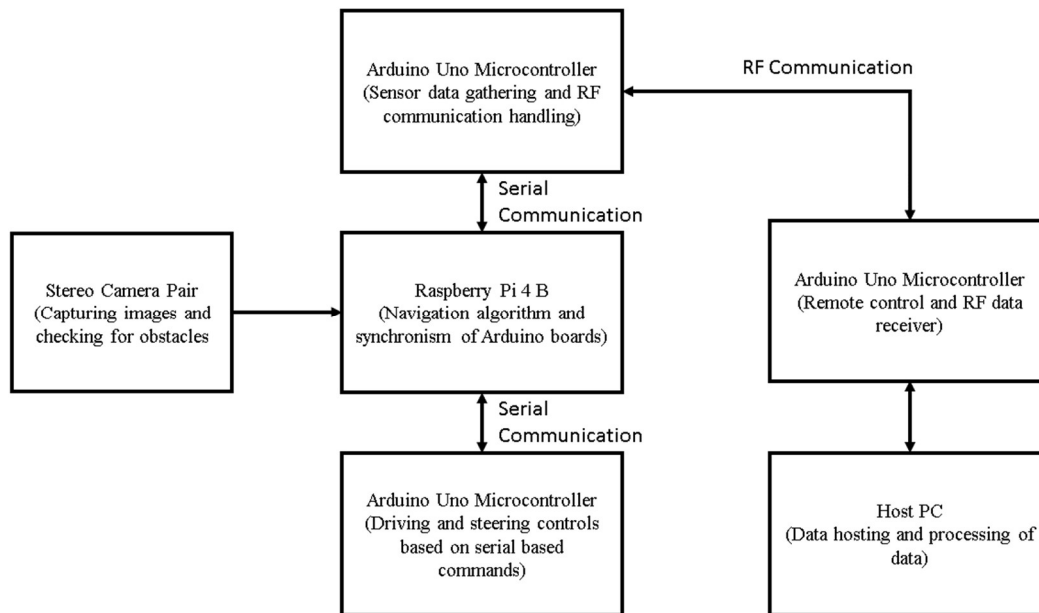


Figure 3.15: Block Diagram showing the various components and their interactions

The Raspberry Pi runs a python script on startup that utilizes several helper functions to communicate with the Arduino Microcontrollers and the stereo camera set-up. All python codes and Arduino sketches are attached with the report supplementary data

The first Arduino Uno or the ‘Driving board’ is connected to 3 L293D Motor Drivers. Each input of the motor driver is connected to one digital output pin. The 3 Enable Pins of each IC are connected in parallel to the PWM pins 3,9,10 of the Arduino respectively. The Arduino is also connected to a 16 channel PWM board to which 4 corner servos are connected. The motors are powered by a 12V lead acid battery. The battery voltage is stepped down to 5V using a buck converter to power the servos, the PWM board and the ICs themselves. Motors are connected between output pins of the IC. Servos are connected to any 4 channels of the PWM board as defined in the code.



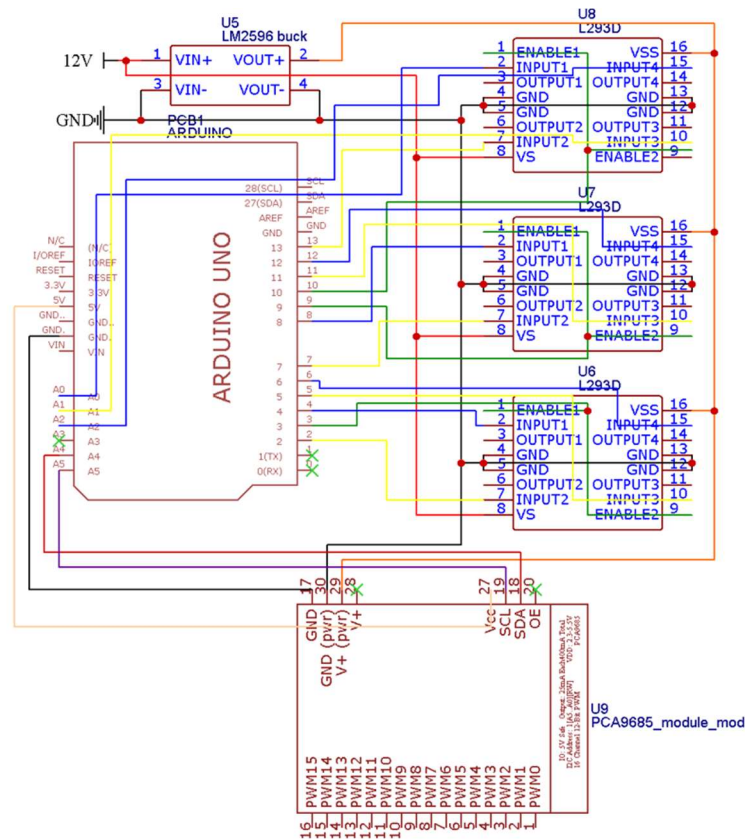


Figure 3.16: Circuit Diagram of Driving Board.

The driving board accepts input via a serial connection to the Raspberry Pi. Commands are sent in the form of numeric codes to the Arduino. Various digits of the command correspond to actions or data required. The first digit of the numeric command conveys what action to undertake whereas the trailing digits after convey information such as what motor combination to use, robot speed required and steering angle to be held.

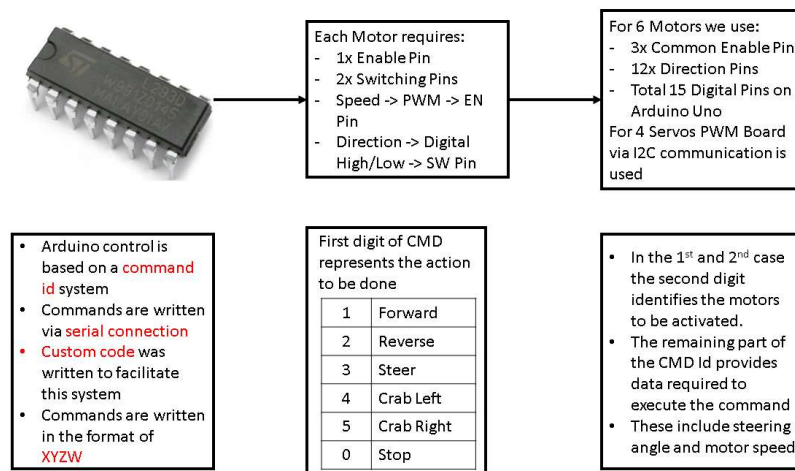


Figure 3.17: Driving board block diagram



The second Arduino board or ‘Control Board’ is connected to the sensors mounted on the rover and the RF chip that sends the information back to the host. This board tracks the operating mode between manual and automatic and appropriately switches the data being sent back and forth between host and bot or between Raspberry Pi and on-board sensors. It performs the processing on the IMU data to convert it into suitable heading and acceleration values that can be used by the rover to solve kinematically the vectors used during navigation. The control board performs its actions by prioritizing serial communication, then RF communication, then requested data as per mode. This order in conjunction with the on-board Raspberry Pi setup and the receiver code ensure that the necessary commands are always sent on time and in the order necessary. 2 sensor connections are used in the prototype, GPS (NEO6M) for geo locating the image, DHT-11 for mapping local temperature and humidity.

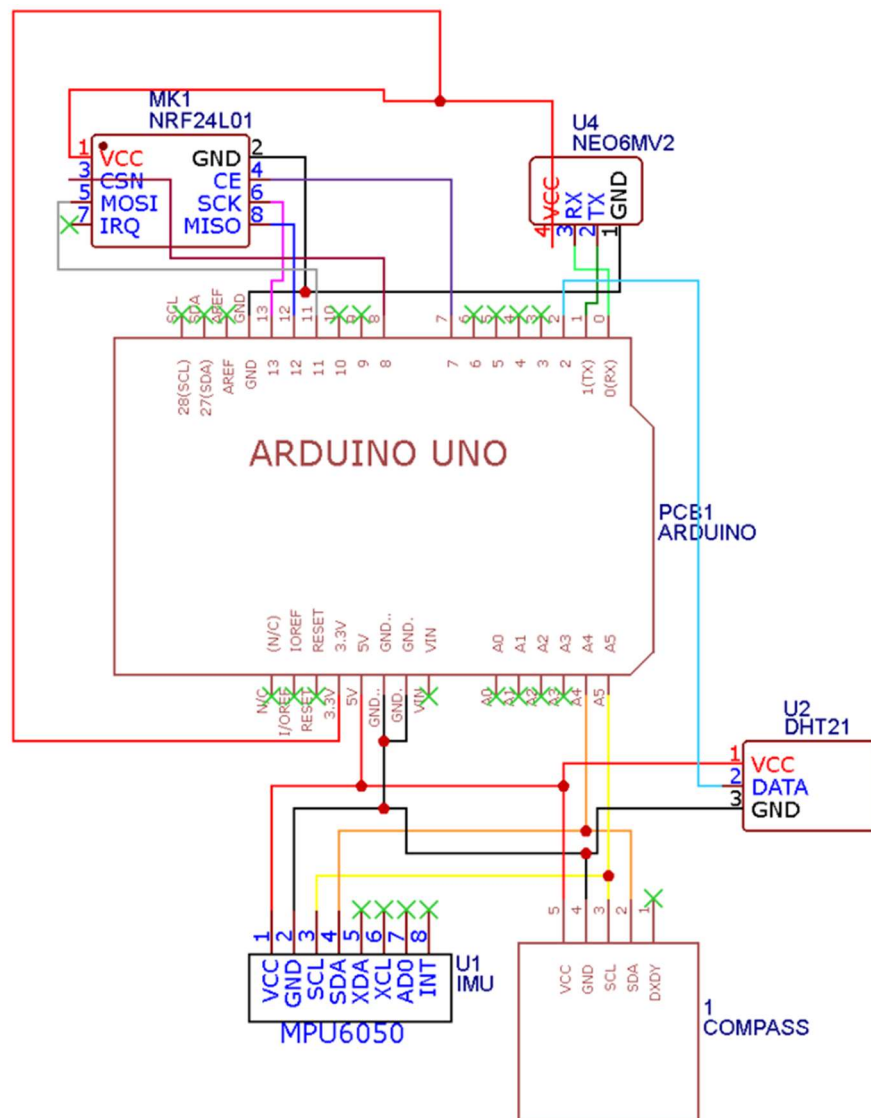


Figure 3.18: Control Board Circuit Diagram

In order to receive the data from the rover, a receiving station is needed. This is accomplished using a third Arduino Uno with an RF module attached to serve as the receiving station. The Arduino also has joystick attached to make driving the rover in manual mode easier for the end user.

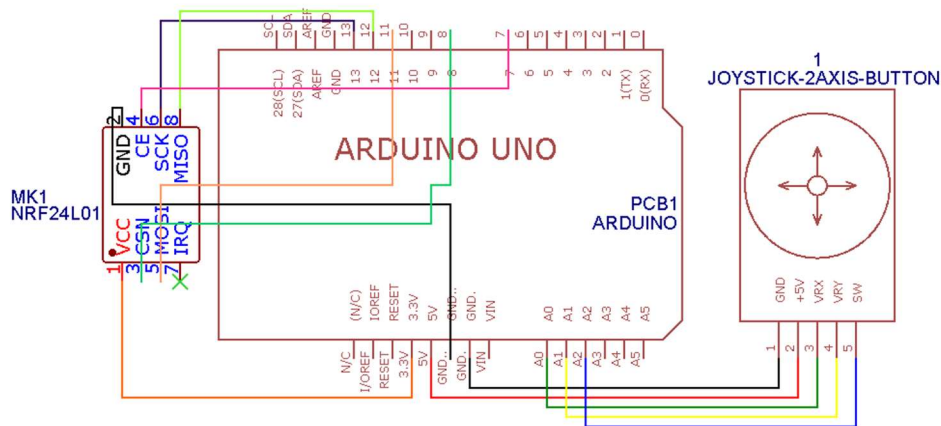


Figure 3.19: Remote Board Circuit Diagram

While the Arduino can handle the processing required to convert joystick inputs into usable commands for rover operations, the data received from both the sensor and image systems needs to be converted into usable data for the end user. This is handled by a python script connected via serial port to the Arduino, allowing for storage of sensor data in csv format and writing images to local drive.

### 3.3.2 Navigational Algorithm

When the rover is operating in its semi-autonomous mode the user can define a target position relative to the rover's current position and the bot will execute the necessary motions required to reach the location. This target position is represented as a vector ( $T_g$ ) in the rover's memory.

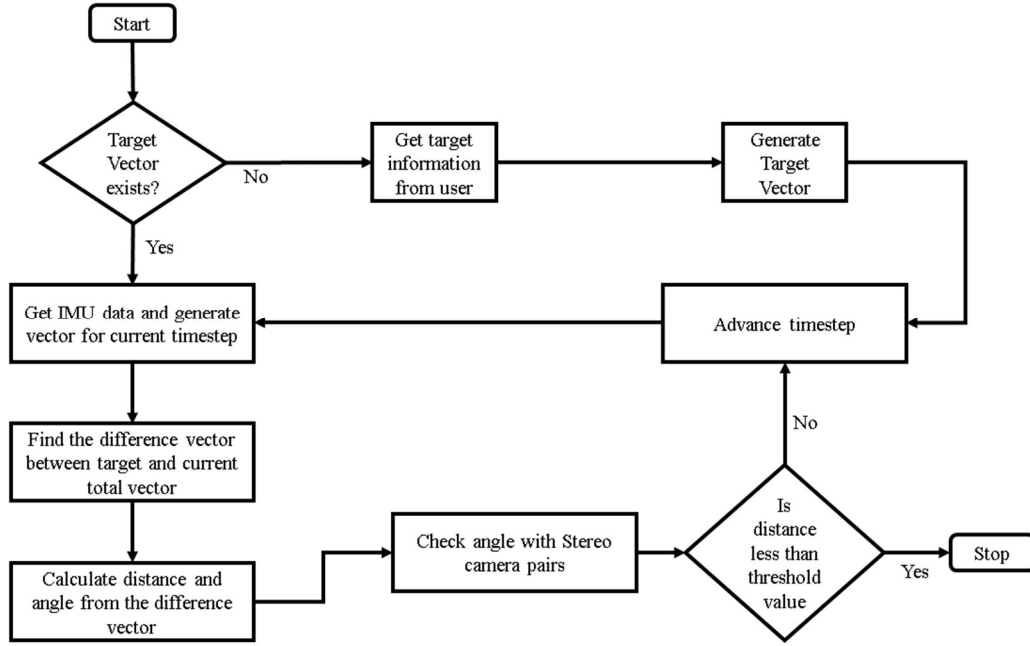


Figure 3.20: Navigation algorithm for rover semi-autonomous navigation

The rover uses its on-board IMU to get the distance and heading travelled. These distances and headings are stored in vector form and a single vector ( $T_t$ ) represents the running tally of the net effect of all the individual vectors travelled. Mathematically it is expressed as,

Equation 3.2: Relation between total vector travelled w.r.t individual vectors from IMU data

$$T_t = \sum_{i=0}^k D_i$$

where,

- $i$  represents any timestep
- $k$  represents the last timestep reached
- $D_i$  is the vector travelled in the  $i^{\text{th}}$  timestep

When each of these vectors are available the following linear combination of vectors can be solved to get a vector ( $R_q$ ) that points to the target position and represents the distance the rover needs to cover and at what heading. With it we calculate the relevant numerical values that guide the rover decision making. Expressed mathematically the equation is,

Equation 3.3: Relation between target, current and required vectors

$$T_g = T_t + R_q$$

where,

- $T_g$  = Target Vector defined at algorithm start
- $T_t$  = Total Vector of all distances travelled
- $R_q$  = Required vector to reach target position

The rover uses a stereo camera pair to detect the obstacles in its path and override the steering angle from the vector calculation to avoid crashing. This system is explained in later in the report. Although this leads to deviation from the path required, this change is reflected in the data acquired by the IMU and thus the system adapts to the change.

### 3.3.3 Stereo Image Computation

Stereo vision is the computation of depth based on the binocular disparity between the images of an object in left and right image [44]. The obstacle avoidance of the robot is performed with the help of stereo vision. Disparity between the left and the right image is the difference between views shown in the two images. A disparity map represents corresponding pixels that are horizontally shifted between the left image and right image [45].

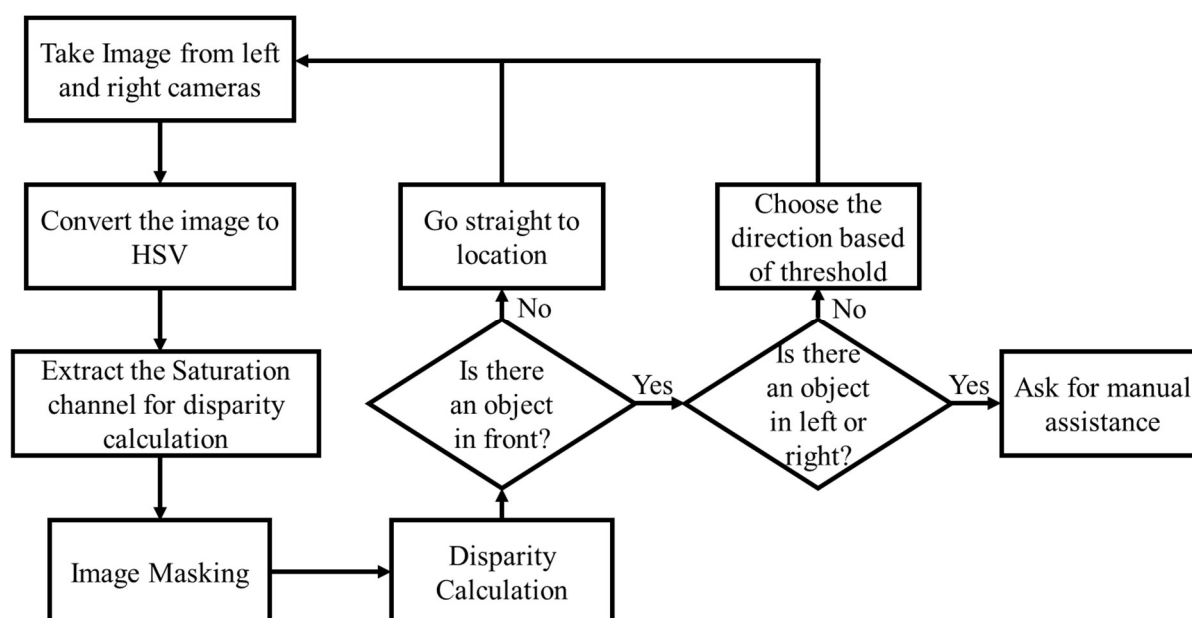


Figure 3.21 Obstacle Avoidance Algorithm

For obstacle avoidance, firstly images are taken by both the cameras. Secondly, these images are in the format Blue-Green-Red (BGR), these are converted to Hue-Saturation-Value (HSV). HSV was preferred over BGR because it is more robust towards external lighting changes. From this, the saturation channel is extracted. Next Image masking is performed. This is done in both left and right images to separate the foreground and the background. The range of saturation channel is from 0 to 255. Hence, from trial and error appropriate value of saturation channel is found out and set as threshold for background separation. In the case of this rover that value was set to 70. Hence all values of saturation channel below 70 were set to 0. The background gets 0 as saturation value corresponding to black color. Thus, in this way the foreground and background are separated.

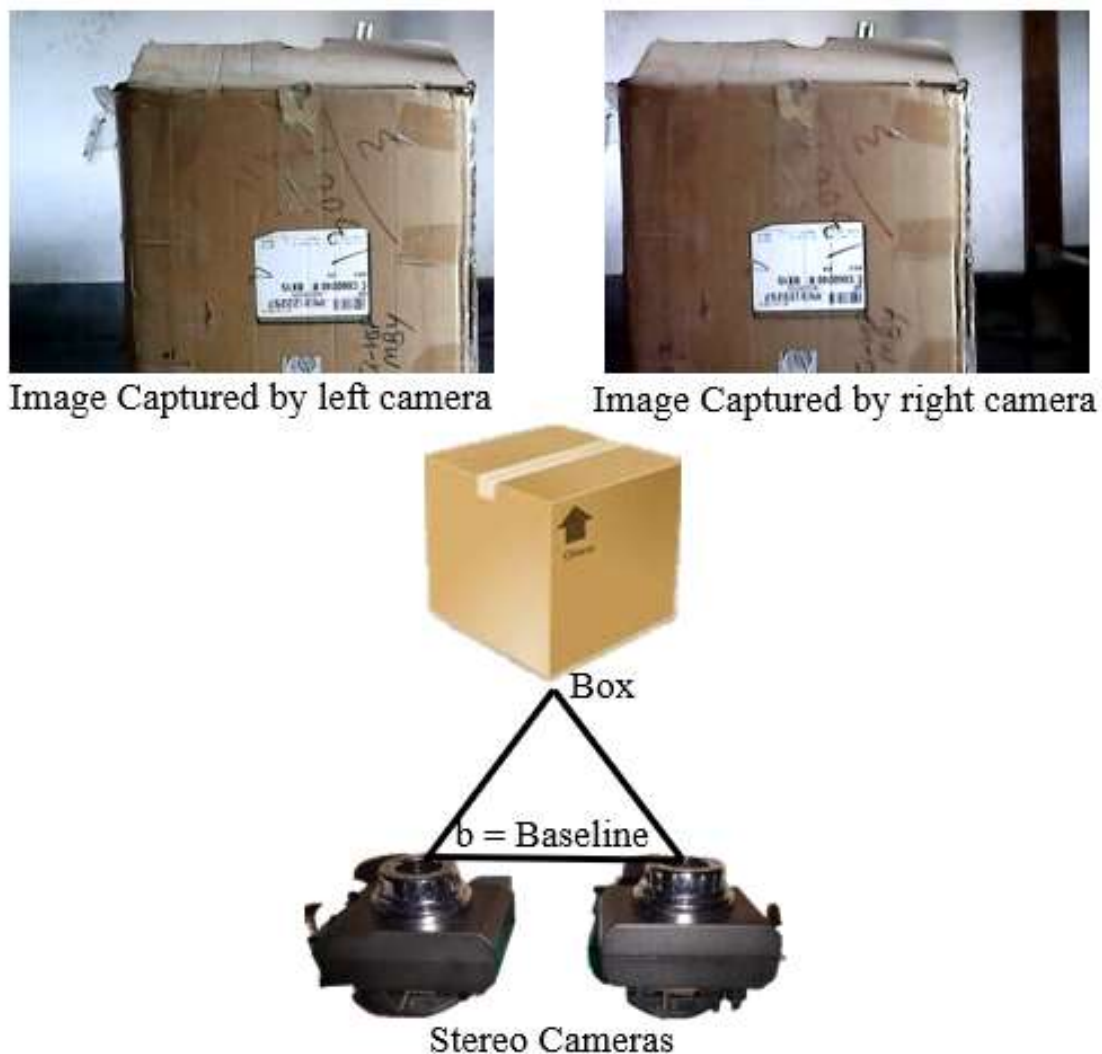


Figure 3.22 Setup to capture reference image

Next, Disparity is found out between the two images in the saturation channel and disparity map is plotted. Now the image is divided into three sections as shown in the Figure 3.23 Disparity Map of Reference Image. First, in the section A of the image the percentage of white pixels are calculated, if the percentage is greater than the threshold i.e, 55% , obstacle is present in the front. Then percentage of white pixels is compared in section B and section C of the image and accordingly decision is take to turn left or right. If it is not possible to take a decision the rover will ask for assistance and switch to manual mode. A reference image (Figure 3.22 Setup to capture reference image) was taken. The box in the image represents an obstacle at a distance of half meter from the cameras. When the above analysis was performed on the following images, it was found that a threshold value of 55% was appropriate for identification of an obstacle i.e., if percentage of white pixels is more than 55% then obstacle is present and vice versa. It can be observed in Figure 3.23 Disparity Map of Reference Image the white pixels are more than 55% in the Section A then the Section B and Section C are tested. In this case even Section B has more than 55% of white pixels but Section C has less than 55% of white pixels. Hence in this case the rover will turn right.

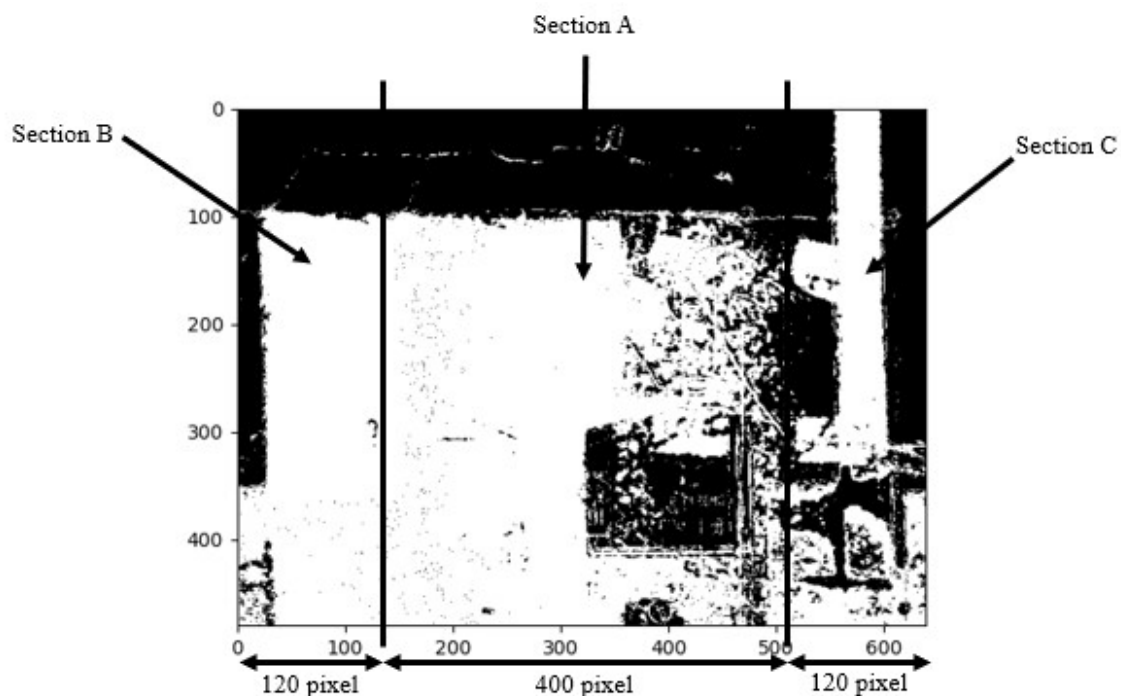


Figure 3.23 Disparity Map of Reference Image

### 3.4 Power and Thermals

Power and Thermals discusses the power requirements of the rover and give a clear view of the electrical circuits that constitute the Rover and how power is distributed from the main source to the individual subsystems.

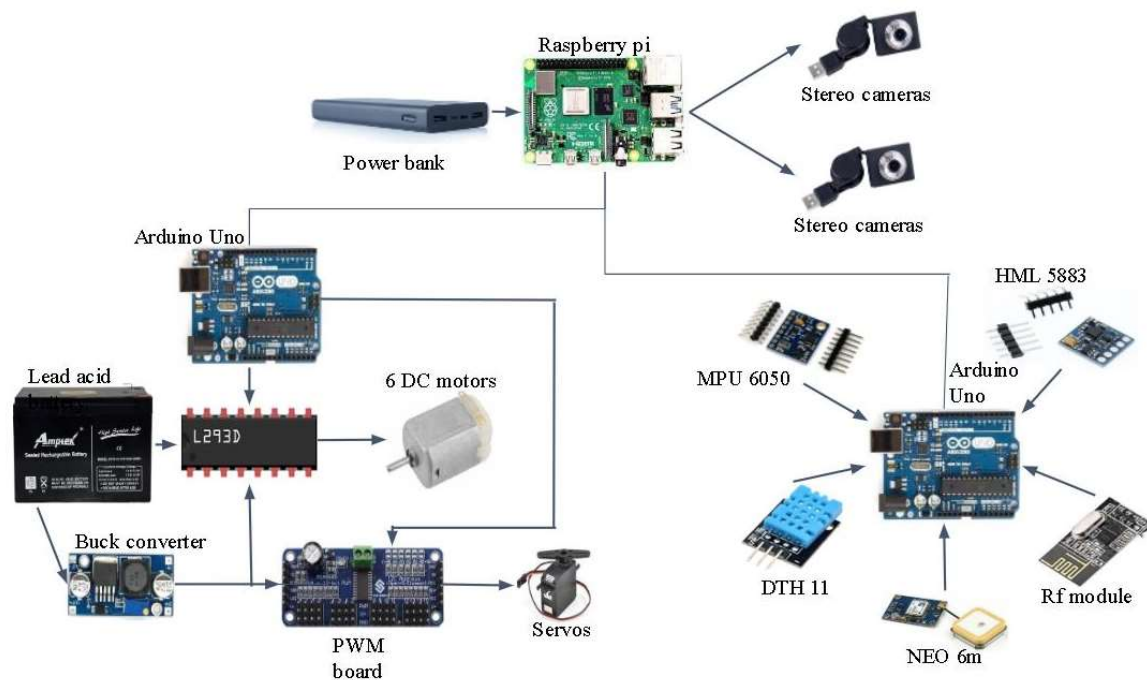


Figure 3.24 Electrical flow diagram

In the above diagram, there are 2 power sources, first, Lead acid battery 12V 1.3Ah and second, a power bank of 20000mAh capacity with a with an output of 5V 2.4A (USB type A) or 5V 3A (USB type C). The majority of power is pulled by DC motors from the 12V Lead Acid battery via L293D IC chip. Lead acid battery also supplies a buck convertor which then steps it down to a 5V which is later a supply for PWM servo board and L293D to run the logic. From the other source (Power bank) Raspberry PI draws power of 5 watts at full load, Raspberry Pi microprocessor is used as a processing unit here, controlling 2 Arduino Uno and processing the Stereo vision and the main code/ program. The GPS requires 3.3V which is provided from the Raspberry Pi and IMU board also requires 3.3V which is provided by the Arduino board.



## Chapter 4

### Implementations and Results

*This chapter discusses the physical prototype built in order to fulfill the project scope and demonstrate the successful application of the domain knowledge*

#### 4.1 Physical Design of Prototype

In order to demonstrate the various objectives of the project, a prototype of the rover was successfully built and deployed. The prototype consists of a main body, a modified rocker-bogie suspension, various sensors and control boards discussed in section 4.3 Control Board, Equipment and Sensor selection of this report and the driving DC motors and servos for steering.

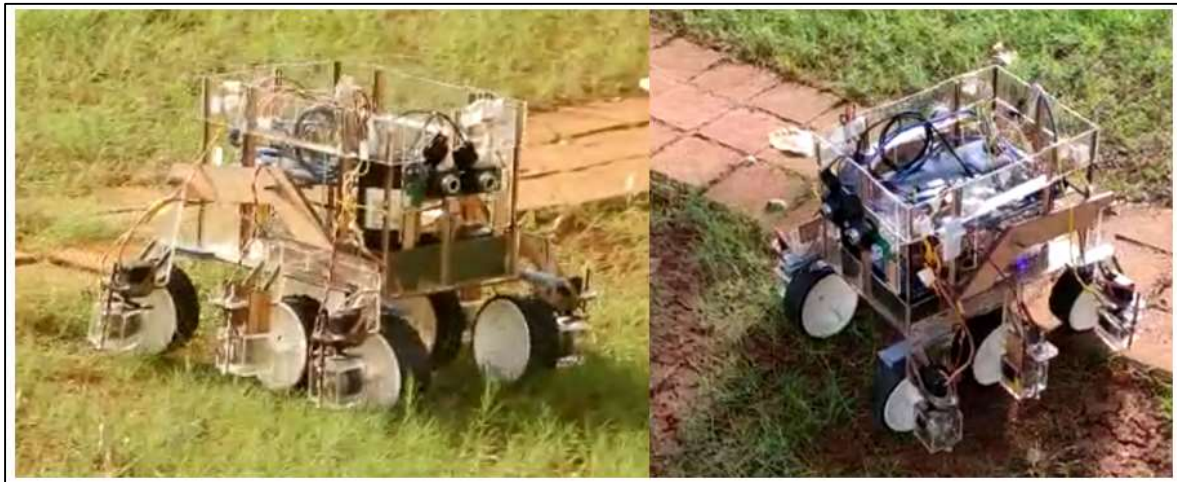


Figure 4.1: Physical Prototype of Rover

The rover's main body is built using acrylic reinforced with ply. Both materials were bought in as sheets and were cut to requisite dimensions using 'Laser Cutting'. The acrylic parts serve as the base part and were sandwiched between sheets of ply where extra strength was required. All parts were cut in a manner that would allow them to slot into each other in a tight fit, thus requiring no jigs or fixtures. The rover uses a cyanoacrylate-based adhesive to adhere these different parts together. In the event of parts requiring higher strength bonding, a two-part epoxy is used to bind them together.



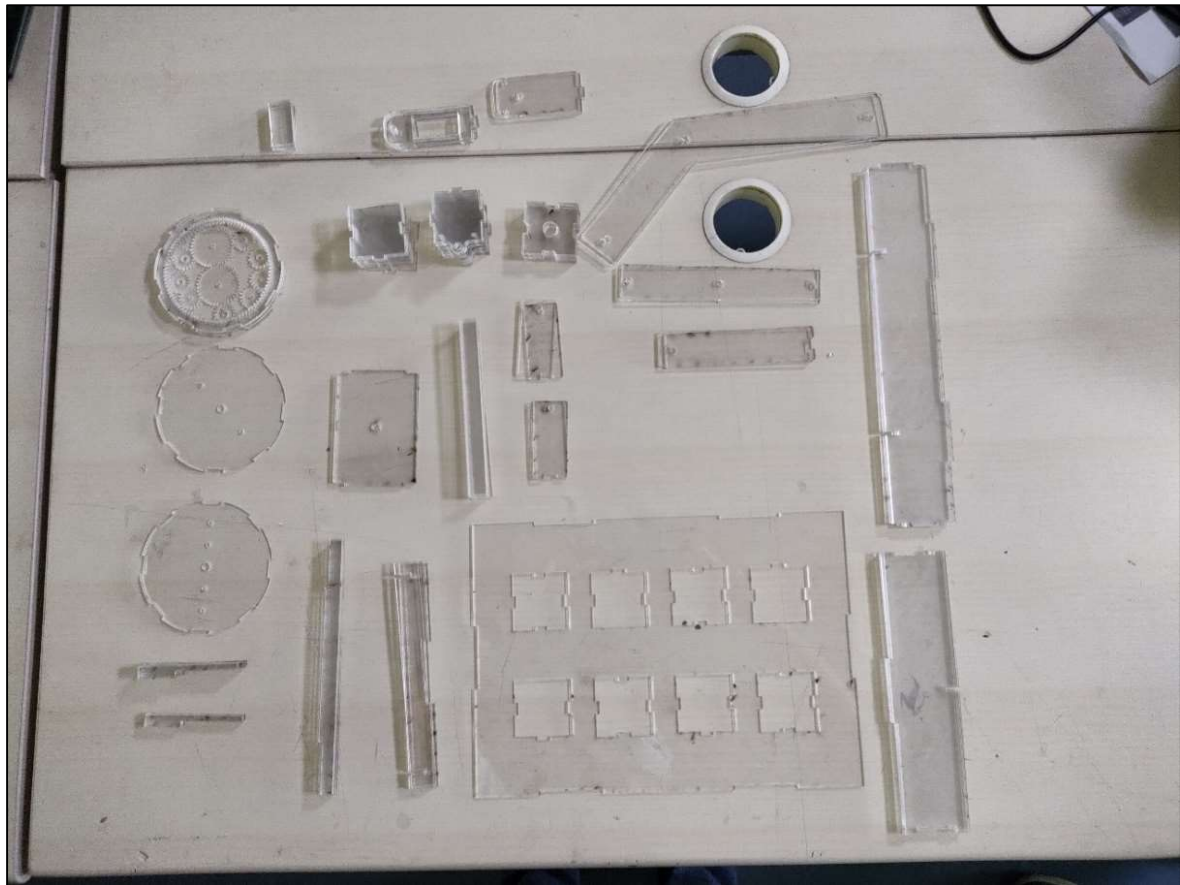


Figure 4.2: Laser Cut acrylic parts of the rover

The suspension follows the rocker-bogie mechanism dimensions, but deviates from the design by mounting rockers on two threaded shafts that bridge across both sides. This deviation in the design was necessary as the differential required for the rocker bogie mechanism would not fit due to the necessary electronics of the rover. The newer suspension is closer to a 3-bogie mechanism which is kinematically similar to the rocker bogie mechanism. This change has not affected the rover's ability to traverse the terrain underneath.

The DC motors driving the rover have their individual cages that secure them using the threads on the motor. The cages are mounted on a threaded shaft that connect them to the rocker-bogie mechanism. The central two wheels are constrained mechanically from rotating. The corner four wheels are connected by a pantograph mechanism to a servo mounted to the ends of the rocker and bogie arms, allowing them to be rotated. All rotations of the suspension and the steering are carried out on threaded shafts secured with nuts. In order to ensure the nuts do not move during rover operation they are locked using thread locker solution.

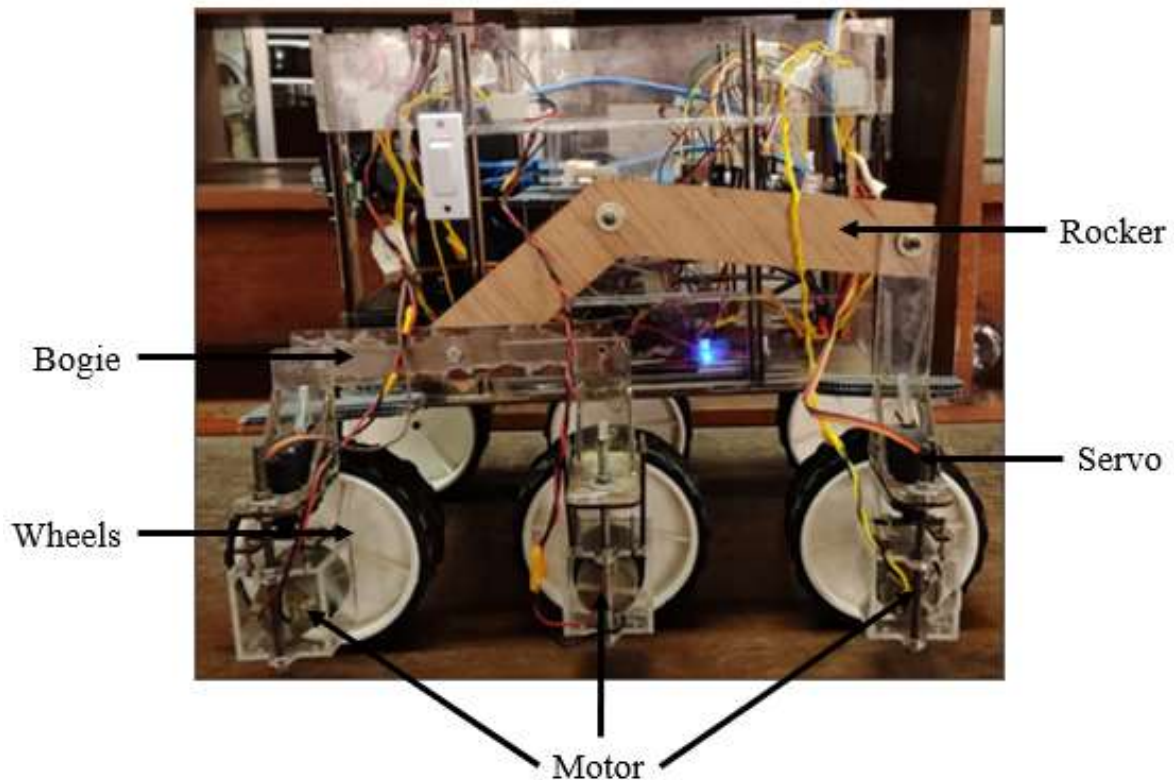


Figure 4.3: Prototype Suspension

The DC motors and Servo PWM board are powered by a 12V 1.3Ah Lead-Acid Battery whereas the Raspberry Pi is powered using a Li-ion Power Bank that then supplies both Arduino's and their sensors as well as the two cameras with the power required via USB. The bi-furcation of the power sources is done purely due to cost constraints of the prototype, with the original plan to power the rover being using a Larger Capacity Lead Acid battery stepped down to 5V and connected to a USB hub to power the Raspberry Pi.

## 4.2 Working of the Prototype

The operations of the rover are coordinated using a python script that runs the main program in a Linux environment. Python as the core language is necessitated due to the use of stereo cameras that require us to use either OpenCV or MATLAB. The board of choice is the Raspberry Pi 4, as it allows for adequate computing power at a reasonable cost. The downside of using the board is that MATLAB is not supported on the Raspberry Pi SoC. Thus, the only choice was to use OpenCV for image processing needs. OpenCV supports both C++ and Python programming languages. Python due to its structure and form lends itself to the prototyping nature of the project. On the receiver end of thing, another Python Script is used

to request and send data, images, switch modes and send target information via the Remote Board.

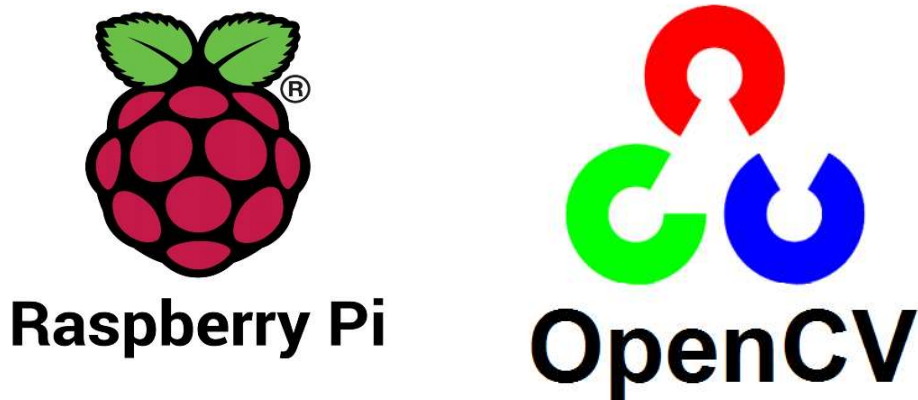


Figure 4.4: Raspberry Pi and OpenCV logos

On startup the rover initializes the Driving Board, by opening a serial connection with it. This will stop all motors and set all servo positions to neutral. Once completed the Driving board will await a command from the Raspberry Pi. The rover will then open a second serial connection with the Control Board, this will initialize the IMU and the RF systems that are necessary for the rover operation. The rover then enters manual driving mode, where the user can drive it around using a joystick connected to the Remote Board and request sensor data and images from the rover. In this mode the joystick position is converted into usable commands and sent via RF to the Rover which then executes them as motion. While the Arduino can handle the processing required to convert joystick inputs into usable commands for rover operations, the data received from both the sensor and image systems needs to be converted into usable data for the end user. This is handled by a python script connected via serial port to the Arduino, allowing for storage of sensor data in csv format and writing images to local drive. The default mode the rover starts in can be changed in the code depending on the use case. The operating mode can be changed via the Remote and follows the algorithm and techniques stated in sections, 3.3.2 Navigational Algorithm and 3.3.3 Stereo Image Computation.






When the user requests sensor data, the python program signals the Control Board, which in turn will collect all sensor data into a single string and transmit it via the RF in a csv format. The prototype currently sends 5 pieces of information over, namely, the temperature, humidity, latitude, longitude and heading of the rover from the on-board DHT-11, GPS and IMU sensors.








This due to the RF sensor being capable of sending only 32 bytes of data at a time. If a powerful communication system is used additional sensors can be accommodated with minor adjustments. Similarly, when the user requests an image from the rover, the Raspberry Pi converts the image into chunks of 8 pixels as csv string that can be sent by the RF. The image is then reconstructed at the receiver by comparing the number of pixels and matching it to the appropriate shape of image required. In the automatic travel mode, the rover executes the both above functionalities automatically once it reaches the target destination.

### 4.3 Control Board, Equipment and Sensor selection

Based on the methodology the selected sensors are outlined in Table 4.1: Electronic Components and its specifications.

Table 4.1: Electronic Components and its specifications

Sensors	Cost (Rupees)	Image	Specification
Raspberry Pi 4	4150		Power: 5V 3A DC via USB-C Processor: Quad core Cortex A72 @ 1.5GHz, 2GB RAM 4x USB ports
Arduino UNO	2100		Operating Voltage: 7V-12V, Number of digital I/O pins: 14, Number of analog input pins: 6
CMOS ¼ Sensor Cameras	800		Max Resolution: 640x480, Aspect Ratio 4:3, FoV: 62° Connection via: USB (VGA)
NRF24L01-Rf module	300		Transmit power: +20dBm, Operating Frequency: 2.4GHz, 6 channels data reception
DC Motor	14400		Rated Speed: 50 RPM, Operating Voltage: 12V, Rated Torque: 392.4 N-cm,

L293D Motor Driver	300		Supply Voltage: 4.5V - 36V Internal logic pins: 5V Can Handle 2 Motors on single IC
MPU 6050 - IMU	500		Input voltage: 3-5V Gyro Range ( $^{\circ}$ /s): $\pm 250$ , 500, 1000, 2000 Accelerometer Range (Gs): $\pm 2 \pm 4 \pm 8 \pm 16$
HML5883 - Magnetometer	250		Input voltage: 3-5V, Operating Temperature: -30 $^{\circ}$ C to +85 $^{\circ}$ C, Communication interface up to 400kHz
DHT 11 Temperature and Humidity Sensor	200		Operating Voltage: 3.3V - 5V, Temperature Range: 0 $^{\circ}$ C to 50 $^{\circ}$ C, Humidity Range: 20% - 90%
NEO 6m - GPS module	340		Supply voltage: 3.3V, Operating Temperature: -40 $^{\circ}$ C to +85 $^{\circ}$ C, Cold start time: 38sec, Hot start time: 1sec
LM2596 – Buck Boost Convertor	80		Input voltage: 3.2-40V, Output voltage: 1.25-35V
Miscellaneous	1580		These include but are not limited to, Fasteners, Solder boards, Soldering equipment, Wires, connectors etc.

#### 4.4 Challenges during prototyping

While manufacturing the prototype rover several challenges were encountered. They arose due to a multitude of factors not limited to, differences in actual properties of material, lack of pre-



existing resources, unexpected behavior of the code. These challenges were overcome to ensure successful completion of the project and safe operation of the rover.

#### 4.4.1 Compass heading changing with orientation

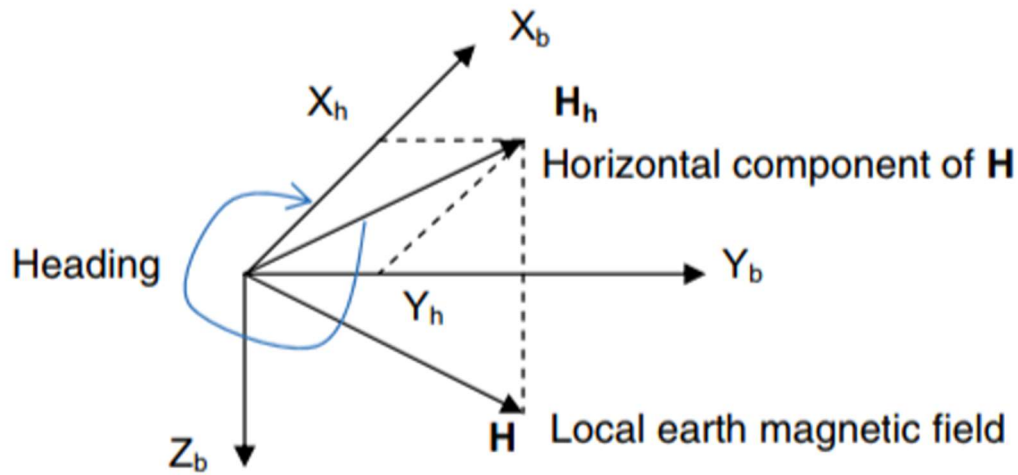


Figure 4.5 Compass heading calculation

QMC5883L/HMC5883L Magnetometer module is used to determine the heading of the rover. However, the default library only considers the effect of the magnetic field in the X and Y axis of the sensor when calculating the heading. This leads to a significant error in the heading, when the sensor is tilted in any orientation not parallel to the ground. In order to correct for this, the pitch and roll values from the 6 axis MPU-6050 must be used in conjunction with the raw X, Y and Z values of the magnetometer to attain a stable heading, regardless of orientation.

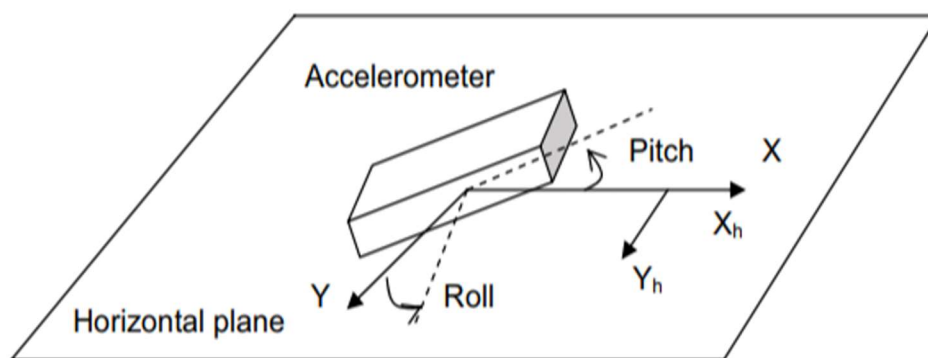


Figure 4.6: Pitch and Roll corrected values for heading calculation

This relation is mathematically quantified as,

Equation 4.1: Equations for pitch/roll corrected heading

$$X_h = X_m * \cos(Pitch) + Z_m * \sin(Pitch)$$

$$Y_h = X_m * \sin(Roll) * \sin(Pitch) + Y_m * \cos(Roll) - Z_m * \sin(Roll) * \cos(Pitch)$$

$$Heading = \arctan\left(\frac{Y_h}{X_h}\right)$$

## Calibrating the Sensor

The sensor was mounted on a rotating platform that could adjust 2 different orientations. Firstly, it's heading parallel to the ground was checked by rotating the sensor by 90 degrees to ensure full 360 degrees of coverage. Then the IMU and the Magnetometer were mounted together onto the platform to ensure correct reading of the magnetometer for various orientations.

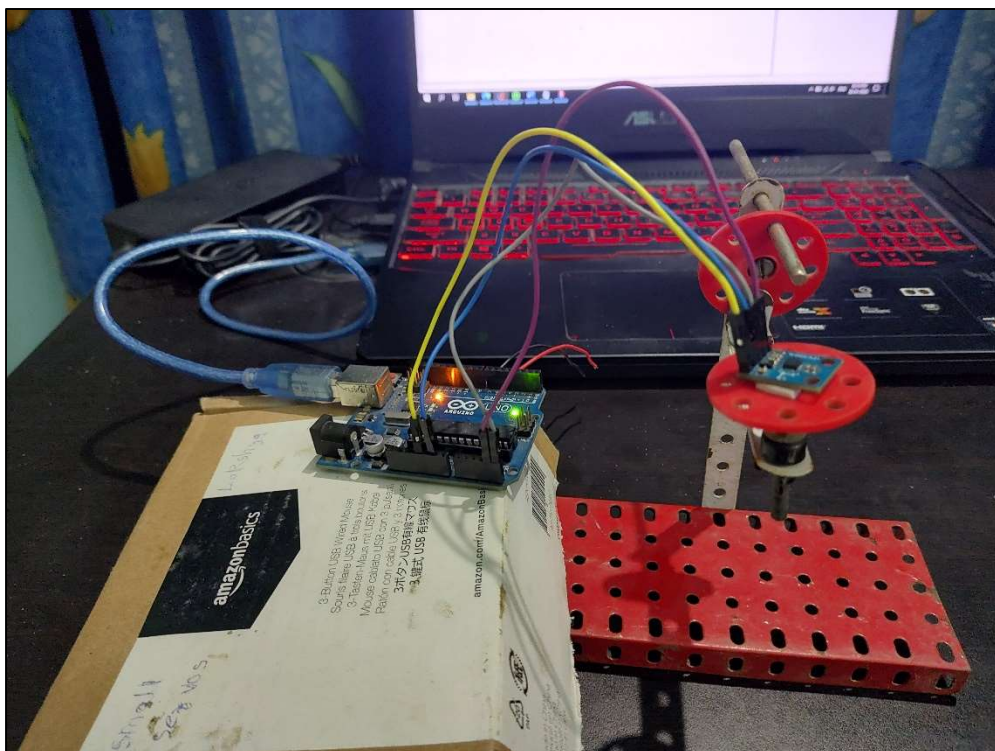


Figure 4.7 Set-up for Magnetometer calibration

#### 4.4.2 Flexure of the prototype during first assembly

After the successful laser cutting of the acrylic parts, a pre assembly check found that there was flexure of components in the suspension. This was caused due to the outward facing wheels of the rover. In order to correct for the same, the amount of ply reinforcement was increased and the orientation of the wheels was switched to face towards the inside of the rover. This would limit the height of obstacles that could be climbed, but would still successfully demonstrate the working principle of the rover and thus was deemed good to change.



Figure 4.8: Flexure of parts during pre-assembly    Figure 4.9: Final bot without flexure

The flexure was also remedied by the servos who held in place the corner wheels thus adding to the stability of the rover. Although the change may appear small, without it the project would have failed.

#### 4.4.3 Powering Servo's from the 12V battery

The PWM board used to power and control the servos connects to the 5V pin of the Arduino via Vcc to power itself and generate the PWM pulse. It however, does not power the 5V pin that is required to run the servo off the board. To do so an additional V+ pin has to be connected to the PWM board. This in turn provides the 5V and current required to run the servos. Since each of the servos on the board can draw up to 200mA of current during operation, it is clear that an Arduino cannot power 4 servos. To remedy the problem, the current from the 12V lead acid battery was used by stepping down the voltage from the battery down to 5V.





Figure 4.10: LM2596 Buck DC-DC Converter

To do so first step-down IC's that could regulate the voltage was used. This was soon whoever deemed risky and prone to failure as several resistors, capacitors and other equipment would need to be added onto the circuit to get a stable 5V output. An easier and compact solution was achieved in the form of a LM2596 Buck-converter that managed to step down the voltage and easily integrate with the 12V circuit. An advantage of this meant that the same 5V line could be branched to power the internal logic of the L293D motor drivers, thus saving on Arduino pins or breadboard connections.

#### 4.4.4 Ineffective Speed Control

During testing of the rover, it was found that the motors did not adhere to the speed setting given to them. The rover's speed is set by turning on and off the Enable Pin on the L293D motor driver using a PWM signal. Originally, Pin 3 of the Arduino was used to generate this PWM pulse and use the same for all 6 Enable Pins. This led to insufficient current on the Pin. Upon the advice of the project guide, the enable pin was split into 3 different pins on the Arduino board to pin 3, 5 and 6. One pin for each pair of wheels front to back. After the change the speed control behavior was observed in the reverse direction for 2 wheels but not the other 4. The code was checked for any variation in the pins but did not spot any. Upon refereeing to the Arduino Uno documentation, it was realized that pin 5 and 6 run at a different PWM frequency, compared to the other PWM pins, hence pins 3,9 and 10 were finalized as the PWM pins on the Arduino Uno. This allowed for full speed control in the reverse direction but not forward. A second check of the code brought into attention that in the forward case the speed control code was not being executed due to the way the C++ handles blocks of code. With minor alterations the issue was corrected and the rover had a fully working speed control on all 6 motors in both directions.

#### **4.4.5 Loss of servo power during rover operation**

While operating the rover it was observed that certain servos would repeatedly fail after reaching turning to one side. This phenomenon is known as servo stall and the servo cuts power to protect itself from harm. This had to be corrected before the rover could be extensively tested. The tests began by, alternating the servos position at lower steering angles (ex 10 to -10), and gradually increasing it to the max steering angle. At lower angles it was observed no such stall phenomenon but as the angle increased the servo would stall. Further investigation also revealed servo jittering caused by the servo reaching its maximum range of motion. It was hence concluded the fault was a combination of poor mechanical mounting of the servo head and excessive trimming of the servos to reflect neutral position. This issue was caused by using the servo library to set neutral during mounting, instead of the PWM board, causing the servo to fall out of sync.

To correct the servo issues, all servos were set to neutral position via the PWM board and remounted them to reflect the same. The upper and lower bound for the maximum steering angle was also reduced in the code by 3 degrees to prevent the servos from stalling.

#### **4.4.6 Stereo Camera defective manufacturing**

For the proper working of stereo vision, some basic stereo camera criteria are to be fulfilled, like there should be 2 cameras (left and right), those cameras should be vertically aligned perfectly, cameras need to have same resolutions size, focus, exposure. When all these criteria are fulfilled, the proper disparity could be obtained so that the depth could be derived out of it. The Stereo camera pair that was ordered was supposed to be of the same model and specifications, instead the two were of the same model but one of the cameras was defective and was not up to the standards. There was severe manufacturing defect, due to which every time the focus was changed, the whole camera rotated internally. Another issue faced was that even the holding clippers of both the cameras were not exactly same due to which a common surface for mounting the camera couldn't be used as vertical alignment of the cameras was required. Another issue faced was that, the defective piece did not have a higher resolution hence the overall quality of the camera was poor due to which it was difficult to get the accurate disparity. A set of images from a different Stereo pair resulted into good disparity concluding the cameras were the short coming and not the code or algorithm.

## Chapter 5

### Conclusions

*This chapter presents the final outcome of our work and possible additions that can be made in the future to add on to the work.*

#### 5.1 Conclusions and results

The working of the rover has been demonstrated using a prototype and hence fulfilling the scope of the project. The working of the following sub-systems has been demonstrated:

- The ability to traverse terrain with bumps and uneven surface.
- Driving of a 6 wheeled, corner steerable rover manually.
- Driving the rover autonomously to the designated target.
- Sending sensor data via RF from the rover to receiver.
- Transmitting images from the rover to the receiver.

It can therefore be concluded that

- The selected rocker bogie design is best suited for the rover as it provides appropriate trade-off between stability, maneuverability, complexity in terms of design and cost of manufacturing.
- The selected microcontroller boards provide appropriate trade-off between complexity, computational power and manufacturing cost.
- Sensor data can be successfully transmitted to a receiver and stored and visualized when required.
- Images can be transmitted from the rover to the receiver. Although the use of low-band RF on the rover leads to slow transmission speeds. These can be alleviated using faster communication methods with higher bandwidth.
- Stereo cameras with an appropriate amount of filtering can detect an obstacle in the path of the rover and can be used to steer around it.
- Hence, it can be concluded that the rover can be used for a variety of scientific survey operations and provide a safe platform to observe areas during times of disaster both without endangering human life.

## 5.2 Further Work

The prototype built although complete can be improved upon and the following points can be used to further improve upon the work presented in this report.

- Integrating the functionality of the driving and control boards onto a singular Arduino board.
- Using better communication hardware such as Wi-Fi, Bluetooth, 4G/5G/LTE to improve the communication speed and increase the amount of data transmitted.
- Optimize the code driving the rover.
- Improve the structure by using metals to fabricate.
- Add insulation and perform thermal study to increase the operating envelope w.r.t ambient temperature.
- Integrate alternate sensors such as LIDAR, 360° cameras instead of Stereo cameras to allow for all round obstacle detection.
- Use of industrial sensors like gas sensors, sound sensors and pressure sensors to monitor large scale processes and remote operations like oil pipeline surveillance
- A cursory study found that solar panels can serve as a good option to increase the range of the rover beyond battery capacity

## References

- [1] W. Thuiller, "Climate change and the ecologist," *Nature*, vol. 448, p. 550–552, 2007.
- [2] P. Stott, "How climate change affects extreme weather events," *Science*, vol. 352, p. 1517–1518, 2016.
- [3] W. Kron, P. Löw and Z. W. Kundzewicz, "Changes in risk of extreme weather events in Europe," *Environmental Science & Policy*, vol. 100, p. 74–83, 2019.
- [4] S. Islam, M. Khan and M. Islam, "Solar PV output under different wavelength of light: A Simulation Based Study," *International Journal of Scientific & Engineering Research*, vol. 9, pp. 1037-1042, February 2018.
- [5] D. Bickler, "The Mars rover mobility system," 1997.
- [6] R. A. Lindemann and C. J. Voorhees, "Mars Exploration Rover mobility assembly design, test and performance," in *2005 IEEE International Conference on Systems, Man and Cybernetics*, 2005.
- [7] G. Udupa and P. Sreedharan, "Design of Spider Mechanism for Extraterrestrial Rover".
- [8] H. P. Moravec, "The CMU Rover.," in *AAAI*, 1982.
- [9] S. Singh, R. Simmons, T. Smith, A. Stentz, V. Verma, A. Yahja and K. Schwehr, "Recent progress in local and global traversability for planetary rovers," in *Proceedings 2000 ICRA. Millennium Conference. IEEE International Conference on Robotics and Automation. Symposia Proceedings (Cat. No. 00CH37065)*, 2000.
- [10] R. Lagisetty, N. K. Philip, R. Padhi and M. S. Bhat, "Object detection and obstacle avoidance for mobile robot using stereo camera," in *2013 IEEE International Conference on Control Applications (CCA)*, 2013.
- [11] X. Guan, X. Wang, J. Fang and S. Feng, "An innovative high accuracy autonomous navigation method for the Mars rovers," *Acta Astronautica*, vol. 104, pp. 266-275, 2014.
- [12] J. Yen, A. Jain and J. Balaram, "ROAMS: Rover analysis, modeling and simulation software," 1999.
- [13] J. Y. Wong, "Predicting the performances of rigid rover wheels on extraterrestrial surfaces based on test results obtained on earth," *Journal of Terramechanics*, vol. 49, pp. 49-61, 2012.

- [14] J. Y. Wong and T. Kobayashi, "Further study of the method of approach to testing the performance of extraterrestrial rovers/rover wheels on earth," *Journal of Terramechanics*, vol. 49, pp. 349-362, 2012.
- [15] T. Hojnik, R. A. Dungavell, P. D. Flick and J. M. Roberts, "Wheeled Rovers With Posable Hubs for Terrestrial and Extraterrestrial Exploration," *IEEE Access*, vol. 8, pp. 154318-154328, 2020.
- [16] H. J. Eisen, C. W. Buck, G. R. Gillis-Smith and J. W. Umland, "Mechanical design of the Mars Pathfinder mission," 1997.
- [17] H. J. Eisen, L. C. Wen, G. Hickey and D. F. Braun, "Sojourner mars rover thermal performance," *SAE transactions*, p. 697-707, 1998.
- [18] R. Roncoli and J. Ludwinski, "Mission design overview for the mars exploration rover mission," in *AIAA/AAS Astrodynamics Specialist Conference and Exhibit*, 2002.
- [19] K. S. Novak, C. J. Phillips, G. C. Birur, E. T. Sunada and M. T. Pauken, "Development of a thermal control architecture for the Mars Exploration Rovers," 2003.
- [20] P. Bhandari, G. C. Birur, D. Bame, A. J. Mastropietro, P. Karlmann, Y. Liu and J. Miller, "Performance of the mechanically pumped fluid loop rover heat rejection system used for thermal control of the Mars Science Laboratory Curiosity rover on the surface of Mars," in *43rd International Conference on Environmental Systems*, 2013.
- [21] P. M. Stella, R. C. Ewell and J. J. Hoskin, "Design and performance of the MER (Mars Exploration Rovers) solar arrays," in *Conference Record of the Thirty-first IEEE Photovoltaic Specialists Conference, 2005.*, 2005.
- [22] C. C. Pazar, "Resource Utilization on Mars," *Journal of Geophysical Research, Planets*, vol. 124, p. 12, 2020.
- [23] I. Vertat and A. Vobornik, "Efficient and reliable solar panels for small CubeSat picosatellites," *International Journal of Photoenergy*, vol. 2014, 2014.
- [24] G. Tina, G. Gozzo, P. Arena, L. Patanè and S. De Fiore, "Design of a robot photovoltaic power supply system," in *4th IASME/WSEAS International Conference on Energy, Environment, Ecosystems and Sustainable Development (EEESD'08), Algarve, Portugal*, 2008.
- [25] M. Q. Raza, M. Nadarajah and C. Ekanayake, "On recent advances in PV output power forecast," *Solar Energy*, vol. 136, p. 125-144, 2016.
- [26] P. E. Bett and H. E. Thornton, "The climatological relationships between wind and solar energy supply in Britain," *Renewable Energy*, vol. 87, p. 96-110, 2016.

- [27] K. V. Vidyanandan, "An overview of factors affecting the performance of solar PV systems," *Energy Scan*, vol. 27, p. 216, 2017.
- [28] S. Pervaiz and H. A. Khan, "Low irradiance loss quantification in c-Si panels for photovoltaic systems," *Journal of Renewable and Sustainable Energy*, vol. 7, p. 013129, 2015.
- [29] A. A. Khamisani, "Design methodology of off-grid PV solar powered system (A case study of solar powered bus shelter)," *Goolincoln Avenue Charleston, IL: Eastern Illinois University*, 2019.
- [30] "UNO R3 | Arduino Documentation | Arduino Documentation," [Online]. Available: <https://docs.arduino.cc/hardware/uno-rev3>. [Accessed 03 06 2022].
- [31] "RaspberryPI models comparison | Comparison tables - SocialCompare," [Online]. Available: <https://socialcompare.com/en/comparison/raspberrypi-models-comparison>. [Accessed 03 06 2022].
- [32] "Oracle spec-HD1213 (1).pdf," [Online]. Available: [https://www.oraclebattery.com/Portals/0/adam/OracleProductGallery/TrkRCIyi\\_0WXLNGWs-O1HQ/Specifications/Oracle%20spec-HD1213%20\(1\).pdf](https://www.oraclebattery.com/Portals/0/adam/OracleProductGallery/TrkRCIyi_0WXLNGWs-O1HQ/Specifications/Oracle%20spec-HD1213%20(1).pdf). [Accessed 03 06 2022].
- [33] "MG995 - Tower-Pro," [Online]. Available: [https://www.electronicoscaldas.com/datasheet/MG995\\_Tower-Pro.pdf](https://www.electronicoscaldas.com/datasheet/MG995_Tower-Pro.pdf). [Accessed 03 06 2022].
- [34] "MG996R Tower-Pro," [Online]. Available: [https://www.electronicoscaldas.com/datasheet/MG996R\\_Tower-Pro.pdf](https://www.electronicoscaldas.com/datasheet/MG996R_Tower-Pro.pdf). [Accessed 03 06 2022].
- [35] "Addicore LM2596 Adjustable DC-DC Switching Buck Converter," [Online]. Available: <https://www.addicore.com/lm2596-module-p/ad281.htm>. [Accessed 03 06 2022].
- [36] "Buy Ublox Neo 6M GPS Module at Low Price In India | Robu.in," [Online]. Available: [https://robu.in/product/ublox-neo-6m-gps-module/#tab-additional\\_information](https://robu.in/product/ublox-neo-6m-gps-module/#tab-additional_information). [Accessed 03 06 2022].
- [37] "Buy HW-127 Compass Module 3 Axis HMC5883L Magnetic Field Sensor," [Online]. Available: <https://robu.in/product/gy-271-hmc5883l-3-axis-electronic-compass-module-magnetic-field-sensor/>. [Accessed 03 06 2022].

- [38] "DHT11 Humidity and Temperature Digital Sensor," [Online]. Available: <https://www.microbot.it/en/product/153/DHT11-Humidity-and-Temperature-Digital-Sensor.html>. [Accessed 03 06 2022].
- [39] "Addicore GY-521 MPU-6050 3-Axis Gyroscope and 3-Axis Accelerometer IMU," [Online]. Available: [https://www.addicore.com/GY-521-MPU6050-p/170.htm#:~:text=Weight%3A%202.1g%20\(0.07oz](https://www.addicore.com/GY-521-MPU6050-p/170.htm#:~:text=Weight%3A%202.1g%20(0.07oz). [Accessed 03 06 2022].
- [40] "Overview of materials for Acrylic, Cast," [Online]. Available: <https://www.matweb.com/search/datasheet.aspx?bassnum=O1303&ckck=1>. [Accessed 24 05 2022].
- [41] D. S. Chinchkar, S. S. Gajghate, R. Panchal, R. Shetenawar and P. Mulik, "Design of rocker bogie mechanism," *International Advanced Research Journal in Science, Engineering and Technology*, vol. 4, p. 46–50, 2017.
- [42] S. S. Rattan, *Theory of machines*, Tata McGraw-Hill Education, 2014.
- [43] P. D. Cenek, N. J. Jamieson and M. W. Mclarin, "Frictional characteristics of Roadside Grass Types, Opus International Consultants," *Central Laboratories*.
- [44] R. Jenny, "Stereo vision and strabismus," *Eye*, vol. 29, no. 2, pp. 214-224, 2015.
- [45] R. A. Hamzah and H. Ibrahim, "Literature Survey on Stereo Vision Disparity Map Algorithms," *Journal of Sensors*, 2016.

## Appendix

All codes used in this project are available publicly under the GNU GPL v3 License at [https://github.com/The-VAE23/IMU\\_SV\\_Rover](https://github.com/The-VAE23/IMU_SV_Rover)